



JGR Space Physics

-

RESEARCH ARTICLE

10.1029/2025JA034414

Key Points:

- A case study of a magnetosheath jet is shown
- The energy conversion terms are calculated as well as the non-Maxwellianity
- At the leading edge a reconnecting current sheet is present while the jet appears to be cooling or expanding

Correspondence to:

O. W. Roberts, owr10@aber.ac.uk

Citation:

Roberts, O. W., Vörös, Z., Settino, A., Koller, F., Raptis, S., Temmer, M., et al. (2025). Energy conversion and exchange in a magnetosheath jet. *Journal of Geophysical Research: Space Physics*, *130*, e2025JA034414. https://doi.org/10.1029/2025JA034414

Received 7 JUL 2025 Accepted 11 NOV 2025

Author Contributions:

Formal analysis: O. W. Roberts, Z. Vörös, A. Settino, F. Koller, S. Raptis Project administration: O. W. Roberts, Z. Vörös, M. Temmer Validation: F. Koller Writing – original draft: O. W. Roberts Writing – review & editing: O. W. Roberts, Z. Vörös, A. Settino, F. Koller, S. Raptis, M. Temmer, C. Simon Wedlund, X. Li, R. Nakamura

Conceptualization: O. W. Roberts

© 2025. The Author(s).
This is an open access article under the terms of the Creative Commons
Attribution License, which permits use, distribution and reproduction in any medium, provided the original work is properly cited.

Energy Conversion and Exchange in a Magnetosheath Jet

O. W. Roberts¹, Z. Vörös^{2,3}, A. Settino², F. Koller^{4,5}, S. Raptis⁶, M. Temmer⁵, C. Simon Wedlund^{2,5}, X. Li¹, and R. Nakamura²

¹Department of Physics, Aberystwyth University, Aberystwyth, UK, ²Space Research Institute, Austrian Academy of Sciences, Graz, Austria, ³Institute of Earth Physics and Space Science, HUN-REN, Sopron, Hungary, ⁴Department of Physics and Astronomy, Queen Mary University of London, London, UK, ⁵Institute of Physics (Heliospheric Physics Research Group), University of Graz, Graz, Austria, ⁶Johns Hopkins University Applied Physics Laboratory, Laurel, MD, USA

Abstract Magnetosheath jets are regions with an extremely large dynamic pressure compared to that of the background plasma. We present a case study of a magnetosheath jet examining energy conversion processes and its interaction with the surrounding magnetosheath plasma. To understand the energy conversion processes we use data from the Magnetospheric Multiscale mission (MMS) to calculate the scalar product of the total current density **J** and the electric field (in the electron flow rest frame) \mathbf{E}' and the pressure strain interaction term $-(\mathbf{P}_{\alpha} \cdot \nabla) \cdot \mathbf{u}_{\alpha}$. Large energy conversion between the fields and flow is observed at the leading edge of the jet where a flow reversal and a strong current is observed. The Walén test suggests that magnetic reconnection may also occur in this region. Significant heating of the electrons through the compressive channel is observed. Within the jet itself, the plasma is cooling, indicative of an expansion of the jet as it evolves. The non-Maxwellianity of the ion and electron velocity distribution functions are calculated using three different measures. The non-Maxwellianity shows spikes for the electrons near the reconnection site, while ions exhibit higher non-Maxwellianity at the front of the jet and a smaller value near the peak of the dynamic pressure. Electrons and ions show similar trends with a time delay, suggesting a relationship between the non-Maxwellianity, indicating the different scale sizes present for both species.

1. Introduction

The magnetosheath is a strongly turbulent environment (e.g., Alexandrova, 2008; Narita et al., 2021; Retinò et al., 2007; Roberts et al., 2018, 2019; Roberts et al., 2022; Vörös et al., 2016), which lies behind the bow shock where the super-Alfvénic solar wind is strongly decelerated because of Earth's magnetosphere. Compared to typical solar wind parameters, the magnetosheath flow speed is lower, the density higher, the ions have higher temperatures, and fluctuation amplitudes are larger (Artemyev et al., 2022; Bandyopadhyay et al., 2018; Chhiber et al., 2018; Lucek et al., 2005; Narita et al., 2021). The upstream foreshock region where the solar wind is magnetically connected to the bow shock is rich in plasma instabilities, large amplitude magnetic waves, and other phenomena (e.g., Wilson et al., 2014a,b; Turc et al., 2019; Zhang et al., 2022; Turc et al., 2023).

Magnetosheath jets are phenomena characterized by local enhancements in the dynamic pressure that are several times larger than the ambient dynamic pressure (Archer et al., 2012, 2013; Dmitriev & Suvorova, 2012; Eriksson et al., 2016; Escoubet et al., 2020; Hao et al., 2016; Hietala et al., 2009; Karimabadi et al., 2014; Karlsson et al., 2015, 2018; Koller et al., 2022; Němeček et al., 1998; Omelchenko et al., 2021; Palmroth et al., 2018, 2021; Plaschke et al., 2020; Preisser et al., 2020; Raptis et al., 2022; Tinoco-Arenas et al., 2022), and can even exceed that of the ambient solar wind (Plaschke et al., 2013). Typically, jets are also cooler than the surrounding magnetosheath plasma (Archer et al., 2012, 2013; Dmitriev & Suvorova, 2012; Hao et al., 2016; Hietala et al., 2009; Karimabadi et al., 2014; Karlsson et al., 2015; Plaschke et al., 2018; Raptis et al., 2020) and have typical sizes of around a tenth to a few Earth radii (Plaschke et al., 2020). When propagating from their regions of generation, jets can impact the magnetosphere, exciting magnetic reconnection (Hietala et al., 2018; Ng et al., 2021), trigger surface waves on the magnetopause (Archer et al., 2013), cause auroral brightenings (Han et al., 2018; Wang et al., 2018) and ground magnetometer responses (Norenius et al., 2021; Wang et al., 2022) and can cause the onset of substorms (Nykyri et al., 2019). Jets have also recently been observed in the Martian and Jovian magnetospheres (Gunell et al., 2023; Zhou et al., 2024). For a detailed review of the magnetosheath jets, the reader is referred to the reviews of Plaschke et al. (2018); Krämer, Koller, et al. (2025). Recent studies by Koller et al. (2022, 2023) have also shown that jets are sensitive to large-scale magnetic structures embedded in

ROBERTS ET AL. 1 of 20

the solar wind, with fewer occurring during coronal mass ejections and more occurring during high-speed streams. The present case study is an example of a jet occurring in a high-speed stream.

Jets are one of the key processes allowing fast and dense plasma flows to reach the magnetopause. As a result, they are essential in understanding the solar-wind magnetosphere coupling. It remains an open question to what extent jets are relevant for injecting energy into the magnetosheath or potentially generating turbulent structures due to the velocity shears between the jet and the surrounding plasma (Karimabadi et al., 2014; Plaschke et al., 2018; Vörös et al., 2023). As jets can travel faster than the magnetosonic speed, some jets (estimated at 13% by Liu, Hietala, Angelopoulos, Omelchenko, et al. (2020)) are associated with a bow wave (H. Liu et al., 2019). Jets with bow waves have been associated with proton and electron acceleration (T. Z. Liu et al., 2019; Liu, Hietala, Angelopoulos, Omelchenko, et al., 2020; Liu, Hietala, Angelopoulos, Vainio, & Omelchenko, 2020; Vuorinen et al., 2022). In the study of a magnetosheath jet by Eriksson et al. (2016), a strong current sheet was observed at the leading edge of the jet and was interpreted to be a result of velocity shears in relation to the jet.

This work for the first time aims to provide a case study of a magnetosheath jet with the Magnetospheric Multiscale mission (MMS) (Burch, Moore, et al., 2016) to investigate possible energy conversion pathways. The MMS mission is ideal for answering these questions since it has multiple points allowing spatial gradients to be calculated at small scales and the necessary time resolution to calculate both the electromagnetic work (Zenitani et al., 2011) and the pressure strain interaction (Roberts et al., 2023; Sarto et al., 2016; Yang, Matthaeus, Parashar, Haggerty, et al., 2017).

2. Data

We use data measured by the MMS spacecraft on the 27th of January 2017 between 08:06:20 and 08:06:55UT when the four-spacecraft tetrahedral constellation was located in the terrestrial magnetosheath at r = (10.8, -3.9, 1.8) Re in the geocentric solar ecliptic (GSE) coordinate system, and had average interspacecraft separations of 6 km. The planarity and elongation (Robert et al., 1998) of the constellation are P = 0.34, E = 0.13, close to a pseudo-spherical tetrahedron, minimizing the errors for gradient calculation (Chanteur, 2000). This is a sub-interval of the burst mode resolution data used by Chasapis et al. (2018) for turbulence analysis.

Data from OMNI (King & Papitashvili, 2005) for the time interval 08:00-08:10UT with 1 minute time resolution are used to estimate the upstream solar wind values. Although not all data points are available from OMNI therefore a mean of this is used. The OMNI data yield a mean solar wind bulk speed and density of 633 km/s, 4.8 cm⁻³, and a corresponding dynamic pressure of 1.6 nPa. The mean magnetic field components are $\vec{B}_{GSE} = (-4.2, 4.2, 2.4)$ nT. The mean cone angle of the magnetic field $\theta = \cos^{-1}\left(\frac{|B_s|}{|B|}\right)$ is moderate or oblique with a value of 49°, and varies between 43° and 61°, and the Alfvénic Mach number is 10.6. This makes identification of low/high cone angle difficult nevertheless this is in the optimal range (30–60°) for jet production for example. Vuorinen et al. (2019). During this time, the THEMIS B and C spacecraft (Angelopoulos, 2009) are also located in the solar wind. The mean parameters estimated from THEMIS are consistent with those obtained from OMNI. The average upstream parameters are characteristic of a high-speed stream of solar wind which have been associated with increased foreshock transient formation (T. Z. Liu et al., 2017, 2018) and are favorable for jet production (Gutynska et al., 2015; Koller et al., 2022, 2023; LaMoury et al., 2021; Plaschke et al., 2013; Vuorinen et al., 2019). Foreshock transients such as hot flow anomalies (HFAs) and foreshock bubbles are frequently observed under such conditions and can produce energetic electrons (Raptis, Lindberg, et al., 2025), while the compressive edge of the HFA, when transmitted downstram it can cause a high-speed jet formation (Archer et al., 2014; Raptis, Lalti, et al., 2025; Zhou et al., 2023).

Figure 1 displays the measured data from the interval. During this period, the MMS spacecraft were operating in burst mode. The ion and electron measurements from the Fast Plasma Investigation (FPI) (Pollock et al., 2016) were measured with time resolutions of 150 and 30 ms, respectively. Having multiple spacecraft available also allows the determination of spatial gradients of velocity fields (e.g.,M. Dunlop et al., 1988; M. W. Dunlop et al., 2002; M. W. Dunlop et al., 2021; Paschmann & Daly, 2008; Paschmann, 1998). Magnetic field data were measured from the fluxgate magnetometer (Russell et al., 2016) with a sampling rate of 128 Hz, and electric fields were measured with a sampling rate of 8.192 kHz from the Spin plane double probes (SDP) and the axial double probes (ADP) (Ergun et al., 2016; Lindqvist et al., 2016).

ROBERTS ET AL. 2 of 20

21699402, 2025, 11, Downloaded from https://agupub.son.linelibrary.wiley.com/doi/10.1029/2025/1A034141, Wiley Online Library on [21/11/2025]. See the Terms and Conditions (https://onlinelibrary.wiley.com/terms-and-conditions) on Wiley Online Library for rules of use; OA articles are governed by the applicable Creative Commons Licensea

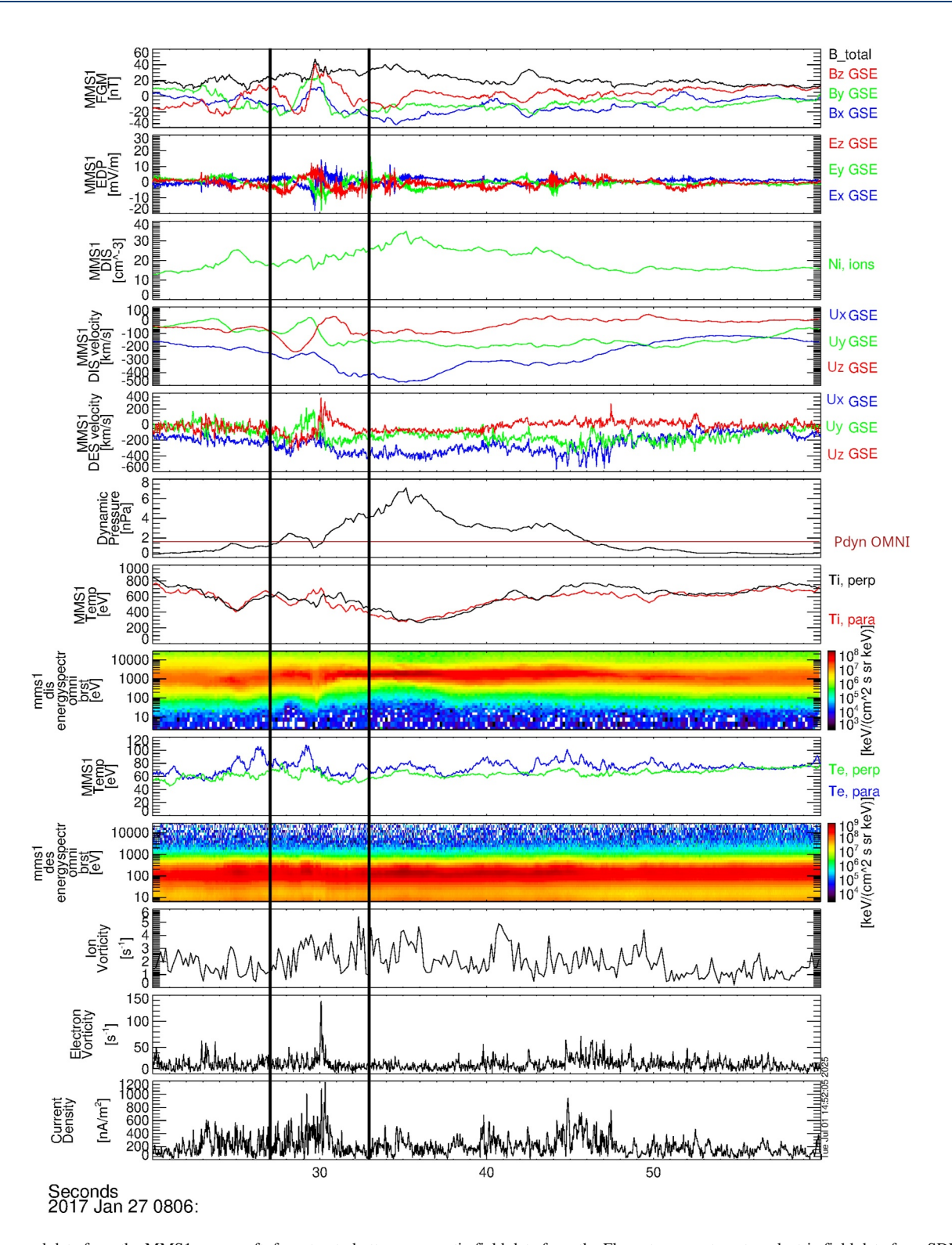


Figure 1. Measured data from the MMS1 spacecraft, from top to bottom; magnetic field data from the Fluxgate magnetometer, electric field data from SDP and axial double probes, ion density from FPI-DIS, ion velocity from FPI-DIS, electron velocity from FPI-DES, ion dynamic pressure $P_{dyn} = \frac{1}{2}\rho u^2$ from fast plasma investigation (black) and the upstream solar wind value from OMNI (red), the ion temperatures (parallel and perpendicular to the mean field) and energy spectra, the electron temperature (parallel and perpendicular) and energy spectra. Finally, the magnitudes of the ion and electron vorticity, and the magnitude of the current density are derived from the curlometer method. The box denotes the sub interval 2017-01-27 08:06:27-08:06:33 where De Hoffmann-Teller analysis has been carried out.

ROBERTS ET AL. 3 of 20

21699402, 2025, 11, Downle

om/doi/10.1029/2025JA034414, Wiley Online Library on [21/11/2025]. See the Terms

At around 08:06:25 UT, an increase in the absolute value of the earthward ion velocity from 200 to \sim 500 km/s is observed. Concurrently, the ion density also increases in this region from 10 to a peak of 30 cm⁻³. Consequently, the dynamic pressure $\frac{1}{2}\rho u^2$ increases drastically in this region from around 1 to a peak of about 7 nPa. During this time, there are high energy ions, the temperature anisotropies of electrons and ions are low, and the magnetic field variance is high, all consistent with a Quasi-parallel jet classification as discussed by Raptis et al. (2020). After the jet the absolute value of the Earthward velocity component (and the dynamic pressure) significantly decreases almost becoming zero, consistent with jets associated to downstream observed HFAs as discussed by Raptis, Lindberg, et al. (2025).

The dynamic pressure measured by MMS between 08:06:30 and 08:06:45UT becomes larger than the solar wind dynamic pressure (1.6 nPa from OMNI). One criteria often used is to define a jet is $\rho_{ms}u_{ms}^2 > 0.25\rho_{sw}u_{sw}^2$ (e.g., Plaschke et al., 2013), which this enhancement satisfies. By comparing magnetic field measurements at each spacecraft, we see that this pressure enhancement travels in the negative x direction (not shown), so that the leading edge is observed first by the spacecraft. Note that the separations sampling rate of FGM is low compared to the advection time; however, the result is also confirmed with the merged Fluxgate search coil (FSM) data (Argall et al., 2018; Fischer et al., 2016) which has a sampling rate of 8.912 kHz.

At the leading edge at 08:06:30 UT, we see an increase in the magnetic field strength, fluctuations in the electric field, some enhancements in the electron parallel (with respect to the mean magnetic field direction) and to a lesser extent, the ion parallel temperature. This is similar to the event of Eriksson et al. (2016). Within the jet, the ion temperature is cooler than the surrounding plasma, which is typically observed for jets (Archer et al., 2012, 2013; Dmitriev & Suvorova, 2012; Hao et al., 2016; Hietala et al., 2009; Karimabadi et al., 2014; Karlsson et al., 2015; Plaschke et al., 2018). The enhanced magnetic field at the leading edge has properties are consistent with the "magnetokinetic" formation mechanism presented in the numerical simulations of Omelchenko et al. (2021), which are supported by the spacecraft observations of Raptis et al. (2022). Observationally jets have a localized turbulent magnetic field enhancement at the leading edge. This pile up allows the shock reformation process to make the faster and less processed solar wind plasma to be observed immediately afterward. Furthermore, at the leading edge of the jet the magnitudes of the current density and electron vorticity are enhanced, and the ion vorticity is fluctuating but slightly elevated. Generally, the electron vorticity has a much larger magnitude than the ion vorticity. The vorticity and current density in this case are measured using the multispacecraft curlometer technique to the velocity and magnetic field respectively (M. W. Dunlop et al., 2002). We will now discuss the possible channels for energy conversion and the two different metrics we use in this work.

3. Energy Conversion Channels

The energy exchange equations for a species α calculated from Maxwell-Vlasov theory can be written as (Yang, Matthaeus, Parashar, Haggerty, et al., 2017; Yang, Matthaeus, Parashar, Wu, et al., 2017):

$$\partial_t \mathcal{E}_{\alpha}^f + \nabla \cdot \left(\mathcal{E}_{\alpha}^f \mathbf{u}_{\alpha} + \mathbf{P}_{\alpha} \cdot \mathbf{u}_{\alpha} \right) = (\mathbf{P}_{\alpha} \cdot \nabla) \cdot \mathbf{u}_{\alpha} + n_{\alpha} q_{\alpha} \mathbf{u}_{\alpha} \cdot \mathbf{E}$$
 (1)

$$\partial_t \mathcal{E}_{\alpha}^{th} + \nabla \cdot \left(\mathcal{E}_{\alpha}^{th} \mathbf{u}_{\alpha} + \mathbf{h}_{\alpha} \right) = -(\mathbf{P}_{\alpha} \cdot \nabla) \cdot \mathbf{u}_{\alpha} \tag{2}$$

$$\partial_t \mathcal{E}^m + \frac{c}{4\pi} \nabla \cdot (\mathbf{E} \times \mathbf{B}) = -\mathbf{E} \cdot \mathbf{J}$$
 (3)

Where, $\mathcal{E}_{\alpha}^{f} = \frac{1}{2}m_{\alpha}\mathbf{u}_{\alpha}^{2}$ is the fluid flow energy of particle species α , $\mathcal{E}^{m} = \frac{1}{8\pi}(\mathbf{B}^{2} + \mathbf{E}^{2})$ is the electromagnetic energy and $\mathcal{E}_{\alpha}^{th} = \frac{1}{2}m_{\alpha}\int (\mathbf{v} - \mathbf{u}_{\alpha})^{2}f_{\alpha}(\mathbf{r}, \mathbf{v}, t)d\mathbf{v}$ is the internal (or random energy). \mathbf{P}_{α} is the pressure tensor, \mathbf{h}_{α} is the heat flux vector, \mathbf{u}_{α} is the velocity, n_{α} is the number density, and q is the charge. Finally, \mathbf{E} and \mathbf{B} denote the electric and magnetic fields and $\mathbf{J} = \sum \mathbf{J}_{\alpha}$ is the total current density.

This system of equations describes the energy conversion processes in a collisionless plasma. Note that the divergence terms on the left-hand side of the equations are transport terms which move energy from one location to the other but do not convert between energy types. We note that often in simulation works the transport terms are assumed to be zero either by integrating over the whole volume and using periodic boundaries (e.g., Yang, Matthaeus, Parashar, Haggerty, et al., 2017). While the magnetosheath is not an isolated system, measurement of these terms (i.e., gradients of heat flux) can have large errors due to being calculated from the third order moment

ROBERTS ET AL. 4 of 20

of the velocity distribution function (VDF) (e.g., Gershman et al., 2015). Nevertheless, the pressure strain terms do tell us about local conversions of energy which is the goal of this work, rather than energy transport or the total energy budget. Conversions in energy between types are through two terms. The first is the $\mathbf{J} \cdot \mathbf{E}$ term, which quantifies the energy conversion between the field and the flow energy (electromagnetic work in a fluid level description). Observationally, a measurement of $\mathbf{J} \cdot \mathbf{E}'$ (also called the Zenitani measure) (Zenitani et al., 2011, 2012) is often used in studies of magnetic reconnection (Bandyopadhyay et al., 2021; Burch, Torbert, et al., 2016; Phan et al., 2018; Torbert et al., 2018), where the prime denotes that the electric field has been transformed into the flow frame of species α .

$$\mathbf{E}' = \mathbf{E} + \mathbf{u}_{\alpha} \times \mathbf{B} \tag{4}$$

Hereafter, we resample the electric field measurements to the electron velocity time tags and we used the pointwise electron velocity (rather than a mean value) to perform the transformation.

$$\mathbf{E}'(t) = \mathbf{E}(t) + \mathbf{u}_{\rho}(t) \times \mathbf{B}(t) \tag{5}$$

The current for species α is given as:

$$\mathbf{J}_{\alpha} = n_{\alpha} q_{\alpha} \mathbf{u}_{\alpha} \tag{6}$$

and the total current density is given as

$$\mathbf{J} = \sum_{\alpha} \mathbf{J}\alpha \tag{7}$$

The current density can be measured directly from the FPI measurements (considering ions and electrons measured by FPI), and the electric field is obtained from the SDP and ADP instruments. For the ion measurements, we resample to the electron time tags and assume that any velocity fluctuations at higher frequencies are much smaller than the electron velocity fluctuations (e.g., Gershman et al., 2018; Roberts et al., 2022).

The second term responsible for energy changes is the pressure strain interaction $-(\mathbf{P}_{\alpha} \cdot \nabla) \cdot \mathbf{u}_{\alpha}$ (Sarto et al., 2016; Sarto & Pegoraro, 2018; Yang, Matthaeus, Parashar, Haggerty, et al., 2017; Yang, Matthaeus, Parashar, Wu, et al., 2017) which can convert energy between the fluid flow energy and the internal energy. This method was previously applied to data from the Magnetospheric Multiscale mission by Chasapis et al. (2017); Bandyopadhyay et al. (2020, 2021) and to simulated data (Pezzi et al., 2019; Yang et al., 2022; Yang, Matthaeus, Parashar, Haggerty, et al., 2017).

The pressure strain term can be further decomposed as follows (e.g., Bandyopadhyay et al., 2021; Yang, Matthaeus, Parashar, Haggerty, et al., 2017)

$$-(\mathbf{P}_{\alpha} \cdot \nabla) \cdot \mathbf{u}_{\alpha} = -p\delta_{ij}\partial_{i}u_{i} - (P_{ij} - p\delta_{ij})\partial_{i}u_{i} = -p\theta - \Pi_{i,j}D_{i,j}, \tag{8}$$

where $p = \frac{1}{3}P_{i,i}$, $\theta = \nabla \cdot \mathbf{u}_{\alpha}$ and $\Pi_{i,j} = P_{i,j} - p\delta_{i,j}$ and $D_{ij} = \frac{1}{2}(\partial_i u_j + \partial_j u_i) - \frac{1}{3}\theta\delta_{ij}$, where δ is the Kronecker delta. Through this decomposition, we can express the pressure strain term as a compressive component $p\theta$, also termed the pressure dilatation, and an incompressive component $\Pi_{i,j}D_{i,j}$. Note that we retain the minus sign here and in the forthcoming plots so that positive values indicate heating. A positive $\mathbf{J} \cdot \mathbf{E}'$ in terms of field particle interactions indicates work done on the particles by the fields (loss of energy by the fields and gain of energy by the particles). Using the multi-point MMS ion and electron velocities and field measurements, both the pressure strain terms and the $\mathbf{J} \cdot \mathbf{E}'$ terms can be evaluated and will now be presented.

4. Results

The largest compression of the magnetic field at approximately 08:06:30 UT is preceded by a local minimum of $|\mathbf{B}|$ and a rotation of magnetic field direction with a duration of less than one second. This suggests the presence of a thin, potentially reconnecting current sheet ahead of the magnetic field that is compressed by the rapidly

ROBERTS ET AL. 5 of 20



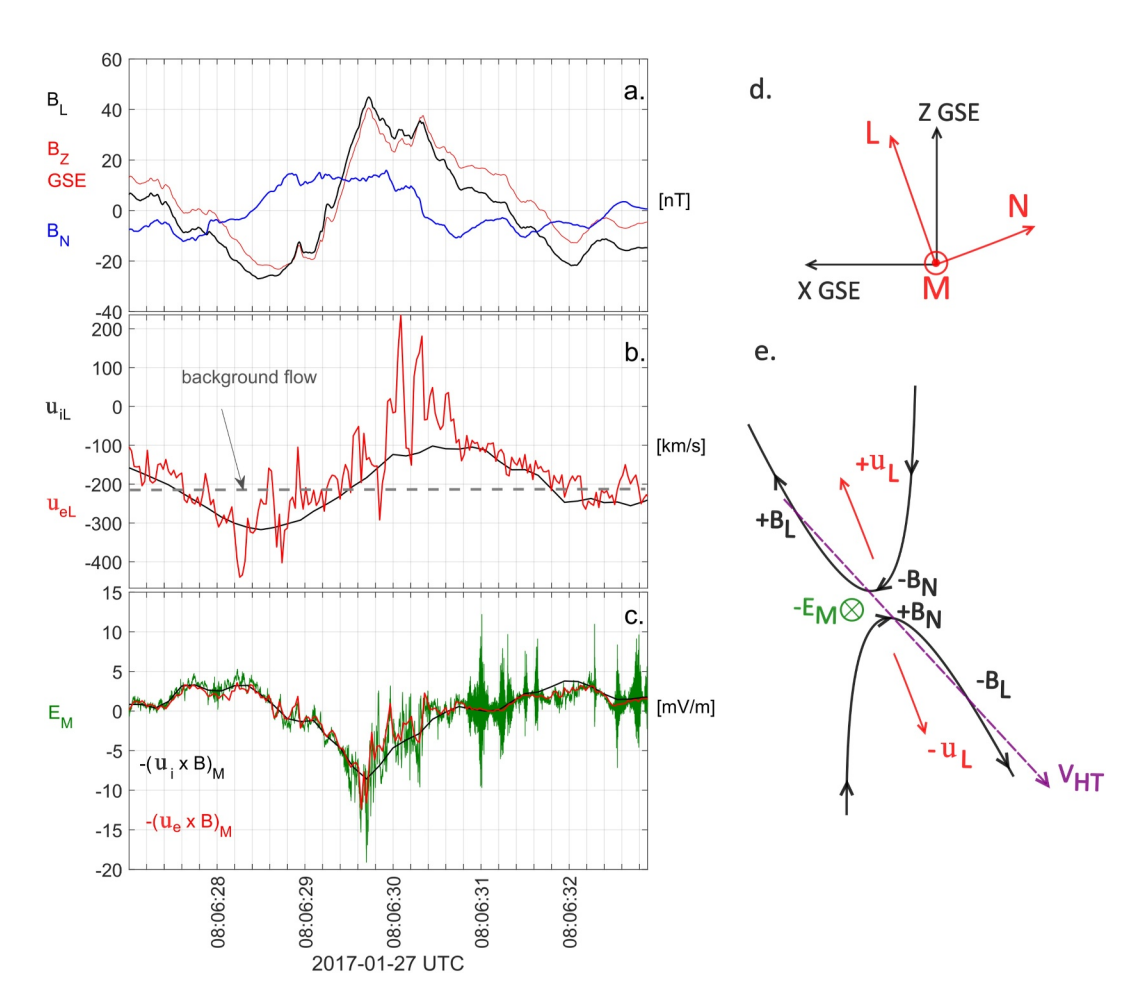


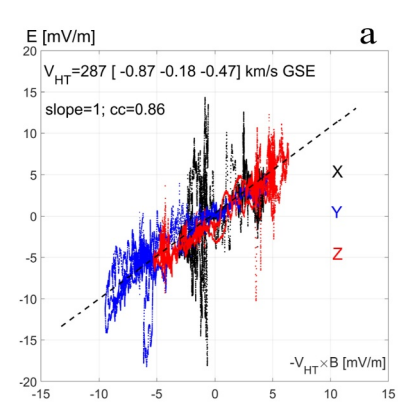
Figure 2. A more detailed look at the boxed area in Figure 1. (a) B_L (black) and B_N (blue) components of the magnetic field. The B_z geocentric solar ecliptic (GSE) component (red) is very close to B_L . (b) Ion and electron outflow velocities, u_{iL} and u_{eL} . The background flow velocity in the L direction is ~ 205 km/s. (c) Out of plane reconnection electric field EM. For comparison $-(\mathbf{u_i} \times \mathbf{B})M$ and $-(\mathbf{u_e} \times \mathbf{B})M$ are also shown. The difference between EM and $\mathbf{u} \times \mathbf{B}$ terms indicate that non-ideal effects take place near the reconnection X line. The ions are more demagnetized than electrons. (d) A cartoon showing X, Z GSE and LMN directions. (e) The reconnecting current sheet is moving with $V_H T$ (Hoffmann Teller) velocity. Because of this motion, the spacecraft first observes $-B_L$, $-V_L$, and $+B_N$, then $+B_L$, $+V_L$ and $-B_N$ values (Figures A A, B). We can see both +L, -L directional outflows because V_{HT} has a significant -Z GSE directional component. So the reconnecting current sheet is moving from +Z toward -Z and toward Earth. The reconnection electric field EM is negative near the reconnection X line.

propagating jet similar to the case study of Eriksson et al. (2016). Magnetosheath jets are known to compress initially thick magnetopause current sheets, thereby enabling reconnection through the dynamic pressure impulse they exert on the magnetopause (Hietala et al., 2018). However, reconnecting thin current sheets and the associated ion/electron outflows are also observed within the magnetosheath itself (Phan et al., 2018; Vörös et al., 2017; Yordanova et al., 2016). In order to determine whether the current sheet in Figure 1 is an undergoing reconnection, minimum variance analysis was performed to the short time interval between 08:06:27- 08:06:33UT which is denoted by the black rectangle in Figure 1 that encompasses the field reversal.

Figure 2 shows this shorter time interval. Minimum variance analysis (Sonnerup & Scheible, 1998) was used to determine the LMN coordinate system where L points in the direction of maximum variance of the magnetic field (in this case it is close to the Z GSE direction.), N points in the direction of minimum variance direction, and M completes the right handed coordinate system. The frame is well determined with eigenvalue ratios of $\lambda_1/\lambda_2=31$ and $\lambda_2/\lambda_3=12$. In the L direction we see a rotation in both the ion and electron flows in Figure 2b with the ion flow changing from ~ -310 km/s to -100 km/s and a background flow of ~ 205 km/s. A comparison of the measured electric field in the M direction (green) and the $\mathbf{u} \times \mathbf{B}$ terms is given in Figure 2c. We see that there are

ROBERTS ET AL. 6 of 20

21699402, 2025, 11, Downloaded from https://agupubs.onlinelibrary.wiley.com/doi/10.1029/2025JA034414, Wiley Online Library on [21/11/2025]. See the Terms



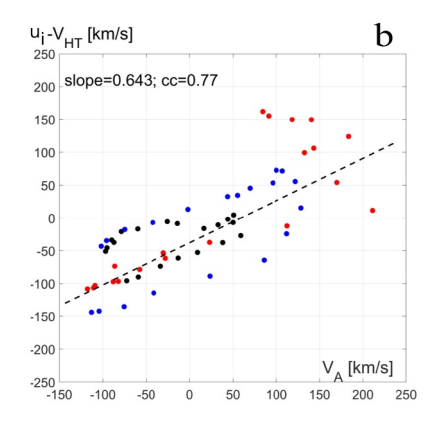


Figure 3. (a) de Hoffmann-Teller frame analysis, the different colors represent the three different geocentric solar ecliptic components, and the dashed line denotes a line with slope 1. (b) Comparison between the $u_i - V_{HT}$ and the Alfvén velocity components. The colors are the same as in (a).

some non-ideal effects where the ions and electrons become demagnetized however they approximate the large scale electric field well.

We found that the local current sheet coordinate system is well determined and the field reversal, or outflow direction is close to GSE Z direction. In fact, the reconnection outflows are seen in $u_{e,L}$ and $u_{i,L}$ components (Figure 2 panels b). A further test for reconnection is accomplished by finding a moving coordinate system, the so-called de Hoffmann-Teller frame (Khrabrov & Sonnerup, 1998), in which the electric field vanishes. If it exists, it can be found from plasma bulk velocity $(\mathbf{u}(t))$ and magnetic field $(\mathbf{B}(t))$ measurements by minimizing the equation $\mathbf{E}_{HT} = -\mathbf{V}_{HT} \times \mathbf{B}$. The velocity $\mathbf{V} = \mathbf{V}_{HT}$ that minimizes the above expression ensures that $|E_{HT}|$ is approximately zero, making the magnetic field structure, in our case the current sheet, stationary. In the HT frame the ion or electron reconnection outflows $\mathbf{u}_i - \mathbf{V}_{HT}$ or $\mathbf{u}_e - \mathbf{V}_{HT}$ should be of the order of the local Alfvén velocity (e.g., Fargette et al., 2023). V_{HT} can be determined from the measured electric field or from the cross products of ion or electron velocities and magnetic field. In Figure 3a the measured electric field components are compared to $-V_{HT} \times B$ components and the minimization of the above expression gives $V_{HT} = 287[-0.87, -0.18, -0.47]$ km/s in GSE coordinates. The scatter of the points around the dashed line with slope = 1 is relatively large, but the average cross-correlation coefficient of the three components is high (cc = 0.86). When instead of the measured electric field $\mathbf{u}_i \times \mathbf{B}$ or $\mathbf{u}_e \times \mathbf{B}$ are used (not shown), \mathbf{V}_{HT} magnitude changes by ~ 20 km/s and the direction by ~ 4 degrees. In Figure 2b the scatter plot of Alfvén velocity V_A and the ion reconnection outflow velocity in the HT frame is shown. The observed slope (cc = 0.643) and average correlation coefficient (cc = 0.766) values are similar to the Walén test results in previously observed reconnection outflows in the magnetosheath (Vörös et al., 2017). These results suggest that we observe an ongoing reconnection in front of the propagating jet.

Figure 4 shows the results of the pressure strain terms, where the magnetic field and the dynamic pressure are shown for context in panels (a) and (b). In panels (c), the value of $\mathbf{J} \cdot \mathbf{E}'$ is shown, where the gray shaded area denotes the uncertainty on the measurement of 0.5 nW/m³ (Ergun et al., 2018). Apart from a small spike at the leading edge of the jet, the $\mathbf{J} \cdot \mathbf{E}'$ is low throughout and smaller than the measurement uncertainty. Panels (d–g) indicate the pressure strain terms, with the lighter shaded areas indicating the measurement uncertainty (Roberts et al., 2023). We use the spin tone product in the moments data to estimate the pressure strain term accurately, removing the spin-related effects from the velocity measurement. We also note some offset in the mean values of the electron velocity's $u_{e,z}$ component. To reduce the effect of this offset on the gradient calculation, we high-pass filter the electron $u_{e,z}$ data before calculating the pressure strain terms. Further discussion of this issue is presented in the Appendix. The final pressure strain terms are separated (Equation 8) so that the compressive electron and ion channels $-p\theta$ are shown in (d) and (f) and the incompressive $-\Pi D$ channels are shown in (g). Throughout the interval, we see that the incompressible ΠD terms are smaller than the compressive $p\theta$ terms. This is often the case in the highly compressible magnetosheath (Bandyopadhyay et al., 2020, 2021; Chasapis et al., 2018).

ROBERTS ET AL. 7 of 20

21699402, 2025, 11, Downloaded from https://agupub.son/inelibrary.wiley.com/doi/10.1029/2025JA0341414, Wiley Online Library on [21/1/12025]. See the Terms and Conditions (https://onlinelibrary.wiley.com/terms-and-conditions) on Wiley Online Library for rules of use; OA articles are governed by the applicable Creative Commons Licensus

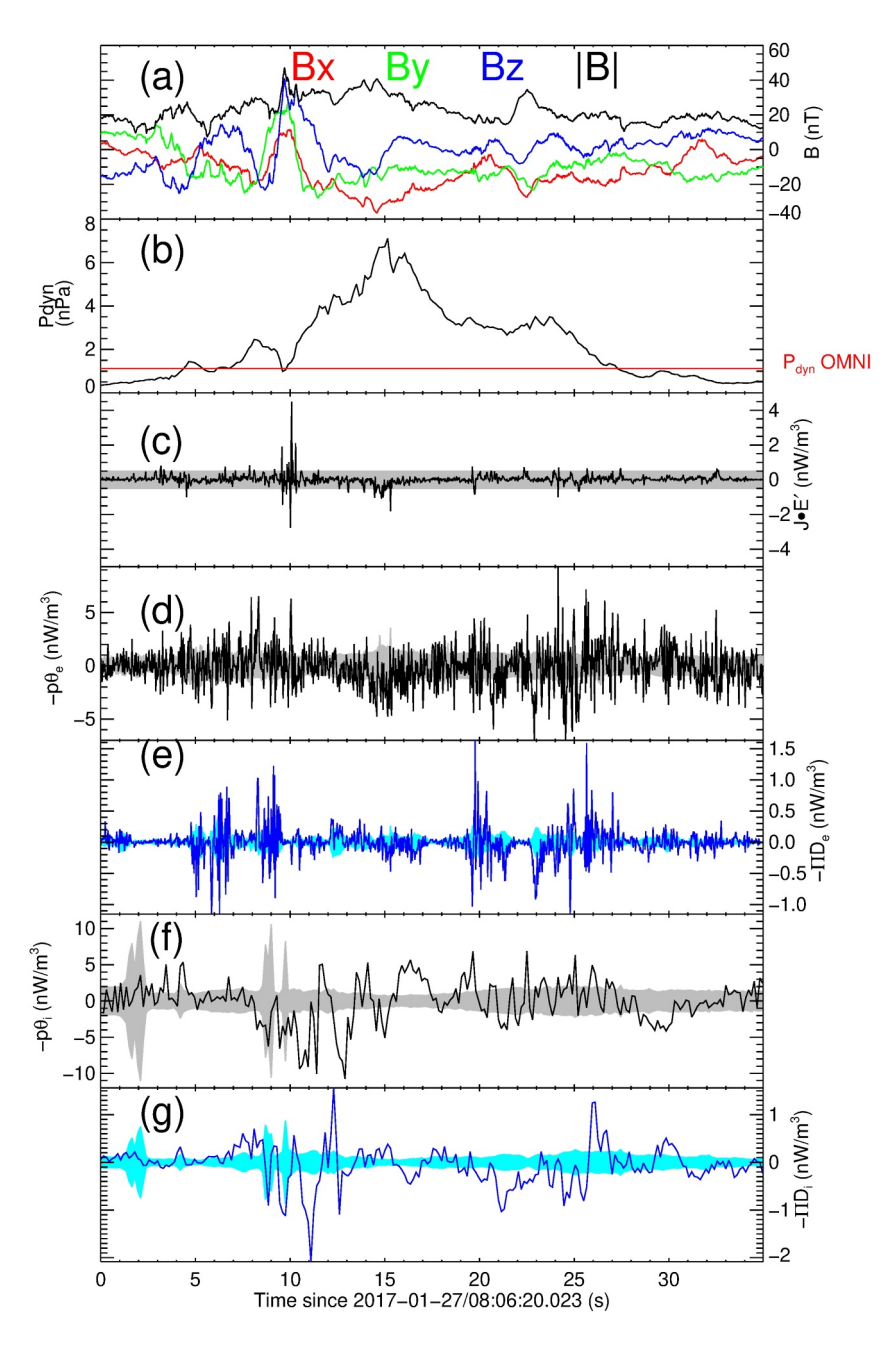


Figure 4. (a) Measured magnetic field data, (b) dynamic pressure are MMS (black) and the upstream solar wind dynamic pressure calculated from OMNI (red), (c) $\mathbf{J} \cdot \mathbf{E}'$ where the shaded area denotes the uncertainty, (d, e) Electron pressure strain interaction separated into compressive ($-p\theta$, panel (d), and incompressive ($-\Pi D$, panel (e). The ion ($-p\theta$, black) (f) and ($-\Pi D$, blue) (g). The gray and cyan areas denote the measurement uncertainty in these quantities.

The relative values of the $\mathbf{J} \cdot \mathbf{E}'$ and the pressure strain terms suggest that for this jet, there is very little conversion of energy between the fields and the flow, while the conversions between the flow and thermal energies are much larger. The exception here is at the reconnecting current sheet where the $\mathbf{J} \cdot \mathbf{E}'$ (Figure 3c) is significant, and is associated with a spike in the $-p\theta$ (Figure 3d) of the electrons. We note that this is the case for this particular jet, other jets associated with wave activity which have been observed for example, by Krämer et al. (2023), would likely also have significant energy conversion in the electromagnetic channels.

An important thing to note here is that both $J \cdot E'$ and the pressure strain terms are fluctuating quantities with field/flow energy and flow/thermal energy continuously being converted between different energy types.

ROBERTS ET AL. 8 of 20

21699402, 2025, 11, Downloaded from https://agupubs.onlinelibrary.wiley.com/doi/10.1029/2025JA034414, Wiley Online Library on [21/11/2025]. See the Terms and Conditions (https://onlinelibrary.wiley.com/terms

and-conditions) on Wiley Online Library for rules

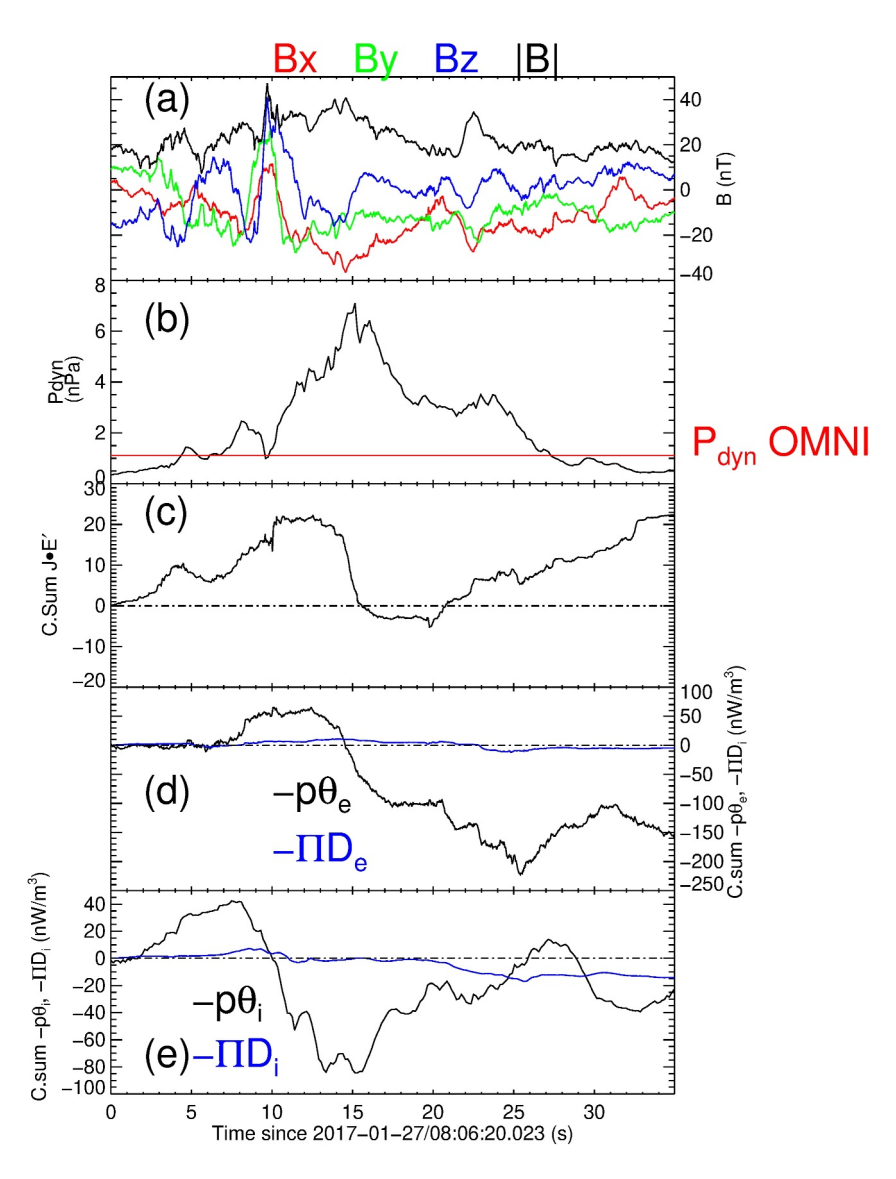


Figure 5. (a) Measured magnetic field data, (b) dynamic pressure from MMS (black) and the upstream solar wind dynamic pressure calculated from OMNI (red), (c) the cumulative sum of $\mathbf{J} \cdot \mathbf{E}'$, (d) cumulative sums of the electron pressure strain interaction terms separated in to compressive ($-p\theta$, black), and incompressive ($-\Pi D$, blue) channels (e) the cumulative sums of the ion pressure strain terms.

However, regarding a given plasma structure, the net energy transfer (instead of instantaneous values) is also relevant. We present the cumulative sums of the different energy conversion measures to measure the net energy transfer in Figures 5c and 5d. The cumulative sum at a point is the sum of all the previous data points so that regions with large or consistent net energy transfers will change while regions with little or no net transfer will remain flat. We point out that these metrics are sensitive to the time resolution, and that there could be transfers of energy with smaller timescales than can be measured, or on spatial scales smaller than the tetrahedron. The tetrahedron scale size is much smaller than the jet size and the time resolution allows many measurement points in the jet. Furthermore, each point in the pressure strain is constructed with moments of the distribution function, therefore we expect net transfer of energy to be described well by these quantities.

The cumulative statistics show very little energy transfer in the incompressible channels for ions and electrons. At the leading edge of the jet, in the cumulative $\mathbf{J} \cdot \mathbf{E}'$ (Figure 4d), we see an initial slight decrease meaning that the fields gain energy in this part, followed by a sharp increase to about 20 nW m⁻³ until the peak of the dynamic pressure where the cumulative $\mathbf{J} \cdot \mathbf{E}'$ reduces. The electron $p\theta$ term shows a strikingly similar evolution to the

ROBERTS ET AL. 9 of 20

 $\mathbf{J} \cdot \mathbf{E}'$ terms, that is, an increase (indicating heating) at the leading edge and then a reduction after the peak. The ion $p\theta$ is generally smaller than the other cumulative metrics, and heating occurs sooner than the other metrics.

To put these results into context we consider the scalar bulk kinetic energy transport,

$$P_{kin} = \frac{1}{2}nm_p u^3 \frac{1}{D} \tag{9}$$

to get a power per unit volume from the bulk flow. For this estimation we assume u = 500 km/s, n = 30 cm⁻³, and D = 800 km (e.g., Plaschke et al., 2020). Using these values, we obtain $P_{kin} \sim 4$ nW/m³. For added context magnetic reconnection have shown energy conversions in the range of $\sim 4 - 20$ nW/m³ (e.g., Bandyopadhyay et al., 2021). The magnetic reconnection observed here is comparable to some of the lower energy cases studied by (e.g., Bandyopadhyay et al., 2021). While this value of ~ 4 nW/m³ may seem small in terms of total energy it is much larger as a cumulative quantity as the energy conversion terms are sporadic, and going between positive and negative. If we consider the cumulative sum of this quantity for the ions for the interval it is +250 nW/m³, which is much larger than the energy conversion terms, and consistent with the majority of energy being in the bulk kinetic energy Krämer, Fatemi, et al. (2025).

To further understand the physics behind the energy conversions observed during this jet event and to identify where does the free energy go, in Figure 6 we investigate distortions of both ion and electron VDFs by means of three different non-Maxwellianity measures, namely,

$$\epsilon_{\alpha} = V_A^{3/2} / n_{\alpha} \sqrt{\int \left(f_{\alpha} - g_{\alpha} \right)^2} d^3 v \tag{10}$$

from Greco et al. (2012) where the background ion Alfvén speed, V_A is used to have a dimensionless quantity. Another definition of non-Maxwellianity used by Graham et al. (2021) is

$$\epsilon_{\alpha}' = 1/n_{\alpha} \int (f_{\alpha} - g_{\alpha}) d^3 v. \tag{11}$$

Finally Kaufmann and Paterson (2009) defined a non-Maxwellianity measure as

$$M_{\alpha} = 2(S_{g_{\alpha}} - S_{f_{\alpha}})/(3k_{B}n_{\alpha}),$$
 (12)

with S being the kinetic entropy density: $S_H = -k_B f H \log H d^3 v$ with $H = (f_\alpha, g_\alpha)$. In the previous definitions, α identifies the particle species, n is the number density, f is the measured VDF, g is the associated Maxwellian distribution with the same density, temperature, and velocity as f_a , and k_B is the Boltzmann's constant. We note that M_{α} is positive definite, having the Maxwellian distribution the maximum entropy. The three measures have been used in a number of plasma environments and simulations (Graham et al., 2021; Greco et al., 2012; Perrone et al., 2024; Pezzi et al., 2021; Richard et al., 2025; Settino et al., 2021). While the measures have yielded similar results when applied to numerical simulations and solar wind data (Perrone et al., 2024; Pezzi et al., 2021), there are subtle differences which capture different physics. The ϵ measure is related to the enstrophy in phase space Servidio et al. (2017); Perri et al. (2020) and scales inversely with the number density Graham et al. (2021). Therefore, when density changes abruptly but plasmas of two different environments and plasmas with different temperatures interact this measure may be affected. The ϵ' measure is not affected by the number density in the same way. Settino et al. (2021) calculated both parameters and good agreement was seen between both measurements during intervals where Kelvin Helmholtz vortices were present and good agreement shows the robustness of the measurement even when density varies. These quantities are also useful as they allow more straightforward comparisons with time series than the VDFs themselves. We also point out that while all three non-maxwellianity measures give information about deviation from a Maxwellian distribution, M_{α} quantifies the contribution of heating/dissipation processes through to the non-Maxwellianity of the VDF. Note that Graham et al. (2021) used a Bi-Maxwellian distribution for the calculations, whereas we use a Maxwellian distribution, however there is very little difference between the results when a bi-Maxwellian or a Maxwellian are used in this

ROBERTS ET AL. 10 of 20

21699402, 2025, 11, Downloaded from https://agupubs.onlinelibrary.wiley.com/doi/10.1029/2025JA034414, Wiley Online Library on [21/11/2025]. See the Terms and Conditions (https://onlinelibrary.wiley.com/terms

-and-conditions) on Wiley Online Library for rules of use; OA articles

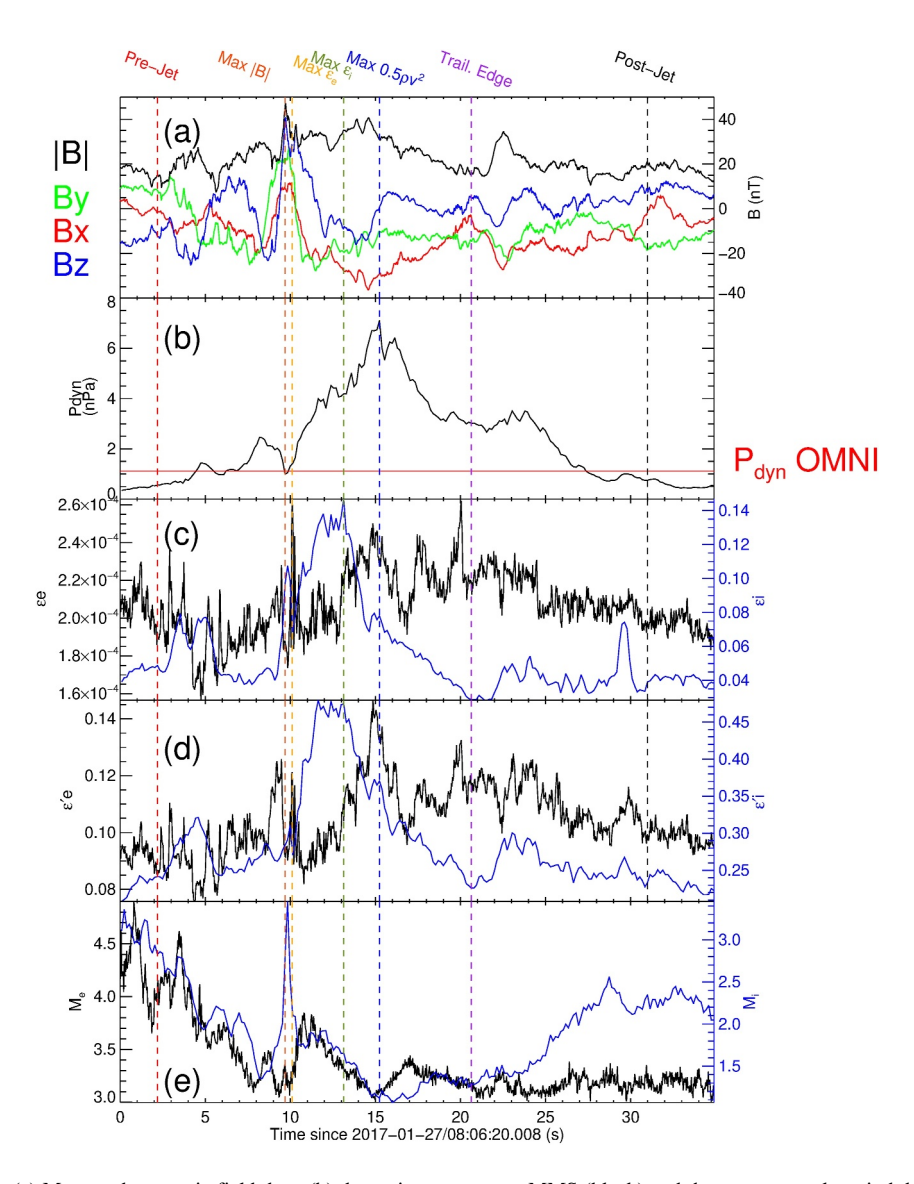


Figure 6. (a) Measured magnetic field data, (b) dynamic pressure are MMS (black) and the upstream solar wind dynamic pressure calculated from OMNI (red), (c) the degee of non-Maxwellianity as defined by Greco et al. (2012) for the electrons (black) and the ions (blue), (d) the degree of non-Maxwellianity as defined by Graham et al. (2021) (e) the non-Maxwellianity measure M as defined by Kaufmann and Paterson (2009). The colored vertical dashed lines indicate times of interest where the velocity distribution functions are shown in Figure 7.

case. This choice was made for consistence as Equations 10 and 12 use Maxwellian distributions. Finally, to reduce the noise associated with the low count statistics, which can artificially increase the non-Maxwellianity (Graham et al., 2021), bins with less than one count have been removed.

A similar trend appears for both e_{α} and e'_{α} in Figures 6c and 6d. At the jet's leading edge, coinciding with peaks in all three magnetic field components ($t \approx 10 \text{ s}$), a localized maximum in electron non-Maxwellianity is observed, while the ion non-Maxwellianity exhibits a local decrease. Concurrently, Figure 5e shows a pronounced increase in M_i , whereas M_e remains low. This suggests that free energy is being channeled into distorting the electron VDFs, while ions undergo significant heating. Between t=10 s and t=12 s, M_e increases, and both e_e and e'_e exhibit local minima, suggesting the onset of thermalization processes affecting electrons, albeit with a temporal delay relative to ions. Within the jet, electron non-Maxwellianities (e_e and e'_e) rise and, despite fluctuations, remain elevated above background levels. In contrast, e_e remains relatively constant and low. A qualitatively similar pattern is observed for ions, though enhancements in (e_i and e'_i) are more spatially confined.

ROBERTS ET AL. 11 of 20

21699402, 2025, 11, Downloaded from https://agupub.son/inelibrary.wiley.com/doi/10.1029/2025JA03414, Wiley Online Library on [21/11/2025]. See the Terms and Conditions (https://onlinelibrary.wiley.com/terms-and-conditions) on Wiley Online Library for rules of use; OA articles are governed by the applicable Creative Commons Licenses

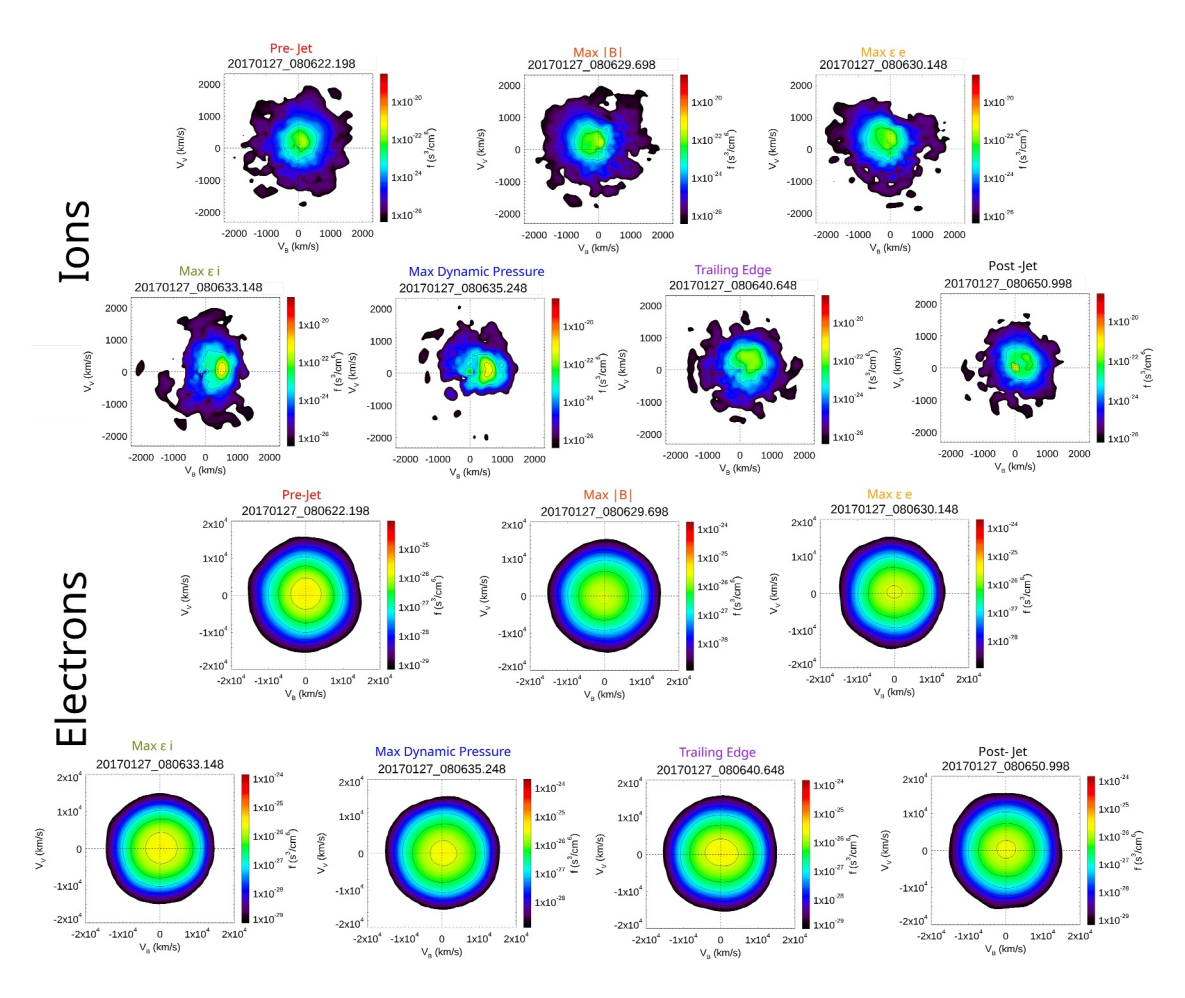


Figure 7. Two dimensional slices of ion and electron velocity distribution functions (VDFs) during the jet event. The VDFs are put in the coordinate system where the magnetic field is in the *x* axis of the plot, which the velocity is in the *x*-y directions. The VDFs are shown for different times of interest which correspond to the dashed lines in Figure 6. We consider the VDFs Pre and Post jet, as well as when the magnitude of the magnetic field has a maximum and when there are local maxima in the non-gyrotropy measure.

Figure 7 shows the VDFs for ions and electrons during the passage of the jet. We have selected several distribution functions at several points of interest which are guided by the measured quantities e.g. dynamic pressure/magnetic field magnitude/non-Maxwellianity. The labels correspond to the dashed vertical lines in Figure 6. The VDFs are put in a coordinate system where the x axis points in the magnetic field direction and the bulk velocity direction is in the x-y plane of the plot. The ion VDFs show minimal non Gaussianity before and after the jet, however in the leading edge where both ϵ values are large there are large distortions in the VDF, and at the moment of maximum dynamic pressure there are two prominent cores for the VDF as was observed also in Blanco-Cano et al. (2020). The differences in the electrons are more subtle, and the non-Maxwellianity measures correspond to VDFs where they become more elongated in the direction of the magnetic field, e.g. at the local Max ϵ_e and at the trailing edge.

Altogether, these observations point to a scenario in which, particles are heated at the jet's leading edge and pushed toward Maxwellian distributions—with ions responding first and electrons following. Within the jet, both ion and electron VDFs remain highly distorted, indicating persistent deviation from local thermal equilibrium. Previous studies have shown that the VDFs of jets deviate from Maxwellian at their onset due to the presence of multiple populations and become more Maxwellian near the dynamic pressure peak. Similar distorsions of VDFs in relation to magnetosheath jets have been observed by Blanco-Cano et al. (2020); Raptis et al. (2022); Blanco-Cano et al. (2023).

We interpret these results as strong compression at the front edge of the jet, and the velocity shears give rise to a reconnecting current sheet in this region. In the region behind this current sheet, the plasma is compressed and

ROBERTS ET AL. 12 of 20

21699402, 2025, 11, Downloaded from https://agupubs.onlinelibrary.wiley.com/doi/10.1029/2025JA034414, Wiley Online Library on [21/11/2025]. See the Terms and Condition

heated, and energy loss from the fields is observed, as well as a gain in energy in the electrons through the compressive energy channel. The ions seem heated slightly before the electrons, possibly due to their larger scale lengths in comparison to the electrons. Jets themselves may have several mechanisms where energy is exchanged with the magnetosheath plasma those that are direct, linked to expansion/compression of the jet and those that are secondary, e.g. reconnection/outflows. After the dynamic pressure peak, cumulative measures decrease, indicating cooling. We interpret this as the trailing edge expanding, thus performing work on the background. There is some evidence from numerical simulations that the sizes of jets do evolve (e.g., Palmroth et al., 2018, 2021) in terms of their size in the x direction from around $0.15 R_E$ to $0.5 R_E$ before contracting (e.g., Figure A1 panel a Palmroth et al., 2021). However, most simulations of jets are two dimensional and the spatial evolution of jets may not be captured fully. Several studies using three dimensions have been performed by a number of authors (Fatemi et al., 2024; Guo et al., 2025; Ng et al., 2021; Omelchenko et al., 2021; Ren et al., 2024). These simulations have highlighted the inadequacy of two dimensional simulations. More complex interconnected jet behavior (e.g., folding/splitting/merging) has been observed by Fatemi et al. (2024); Ren et al. (2024); Guo et al. (2025) when a realistic size of the Earth's magnetosphere is also considered. Together this highlights the need for both three dimensional simulations that also have realistic sizes of the Earth's magnetosphere to capture the relevant physics. It is not straightforward from spacecraft observations to demonstrate that jets are expanding. However, the often observed colder temperature and the local measure from the pressure strain terms suggest this. Detailed comparisons of spacecraft data and simulations with three spatial dimensions may be useful in fully understanding the spatial evolution of jets.

5. Summary and Discussion

To summarize, we have presented a case study of a magnetosheath jet to understand the associated energy conversion and exchange with the magnetosheath plasma. The Pressure strain method is unique and has allowed us to investigate the properties of jets in a completely different and new way. Heating and cooling are predominantly seen in the compressive energy channels, with transfer through the incompressible channel being very small in terms of instantaneous values and cumulative sums. This is generally the case for observations in the magnetosheath (e.g., Bandyopadhyay et al., 2021). Fluctuations in the $\mathbf{J} \cdot \mathbf{E}'$, and $p\theta$ are seen to increase at the leading edge of the jet. The cumulative sums show that at the leading edge, there is a net loss of energy from the fields, which could convert energy to fluid flow energy. At roughly the same time, there is a net transfer of fluid energy to the internal energy of electrons and, to a lesser extent, the ions. We propose that this is due to the velocity shear at the front of the jet, consistent with Eriksson et al. (2016).

Within the jet, the jet is seen to be cooling; several observations of jets have shown that the temperature of jets tends to be smaller than the surrounding plasma. This cooling could hint that during the evolution of the jet, it expands. According to the simulations of Omelchenko et al. (2021), the sporadic formation of high speed jets at foreshock-shock transitional region are due to the compressed solar wind plasma. In this process turbulence, kinetic physics of shock reformation, turbulent convection of magnetic field lines are taking place resulting in plasma filaments of enhanced density. The increasing dynamic pressure anti-correlates with the ion temperature and the temperature is lower than the surrounding plasma when the jets are formed. However, this does not exclude the possibility that the jets continue to expand and cool during their propagation through the magnetosheath. The cumulative sums also show that there is heating at the leading edge of the jet with ions being heated further upstream than the electrons consistent with the characteristic scales of ions being larger than those of electrons. The non-Maxwellianity of the VDFs has also been investigated, and the results reinforce what the pressure strain methodology sees with the ions being affected first and the electrons following. One conclusion of Graham et al. (2021) is that non-Maxwellian VDFs are not typically correlated with local processes. Although the observations of Graham et al. (2021) also suggest higher non-Maxwellianities in the turbulent magnetosheath, and jets likely represent one method of injecting energy into the magnetosheath (e.g., Krämer, Fatemi, et al., 2025).

Due to the limited number of spacecraft examining jets' evolution in situ is very difficult requiring fortuitous alignments of multiple spacecraft. One possibility is to investigate numerically simulated data from simulations with three spatial dimensions so that the evolution can be seen. Virtual spacecraft could also be flown through the simulation to see how metrics such as the pressure strain terms behave when jets evolve to give complete information.

ROBERTS ET AL. 13 of 20

21699402, 2025, 11, Downloaded from https

viley.com/doi/10.1029/2025IA034414, Wiley Online Library on [21/11/2025]. See the Term

and-conditions) on Wiley Online Library for rules of use; OA articles are governed by the applicable Creative Co

Finally, we remark that these conclusions apply to this particular jet and this behavior may not be typical. This jet is an example where the increase in dynamic pressure is driven predominantly by the change in velocity rather than density. Therefore velocity gradients which are calculated in the pressure strain terms may be larger than density driven jets. The interactions may differ for a jet where the velocity is comparable to the background magnetosheath bulk speed. A logical next step would be to investigate many jets; this would be possible using the jet list compiled by Raptis et al. (2020) which covers the years 2015–2020. Although this data set uses predominantly the fast survey mode, a burst survey mode data flag is included. For the pressure strain method burst survey mode is preferable as we usually see spikes, a such as those related to magnetic reconnection that have timescales much shorter than the fast survey mode time resolutions. Another possibility for future investigations is to investigate three dimensional numerical simulations and virtual spacecraft observations of the pressure strain terms and then to compare them to the spacecraft data.

Appendix A: The Need to Filter the u_z Component of the Electron Velocity

In Table A1 we present the mean and standard deviations values of the ion and electron velocity components, and their associated errors. The means of the different particle species would be expected to be similar as the global mean (30 s) is longer than the characteristic timescales. When comparing smaller scales for example, point to point values we would expect differences as ions begin to demagnetize at the ion inertial length.

All components agree nicely with one another except for the electron V_z component which varies from -27 to -43 km/s between spacecraft. It should be noted that the mean statistical error (Gershman et al., 2017) is roughly 8 km/s Figure A1 shows the V_z components of the electron velocity. A slight difference in offset can be seen between the spacecraft which is consistent throughout the interval. A systematic error in the offset will affect the gradient calculation used when calculating the pressure strain terms. To overcome this limitation we high-pass filter the u_z at 0.055 Hz to reduce the effect of the offset data before calculating the terms. In Figure A2 we present the electron pressure strain terms without the high-pass filtering a,b, while c,d shows where we have filtered. When looking at the instantaneous values it is not clear that there is much different, but when we look at the cumulative sums it is clear that a systematic error propagates into the pressure strain terms. When no filtering is applied the cumulative sum shows a clear increasing trend, which we interpret as being due to this offset. We note that this will be case dependent. For studies where the point-wise values of pressure strain is used in extreme cases (e.g., during magnetic reconnection) the systematic error is likely to be insignificant. However, when averages are used the effect may be more pronounced. Therefore some caution is required when using multi-spacecraft gradient methods, and mean values of all parameters should be checked beforehand.

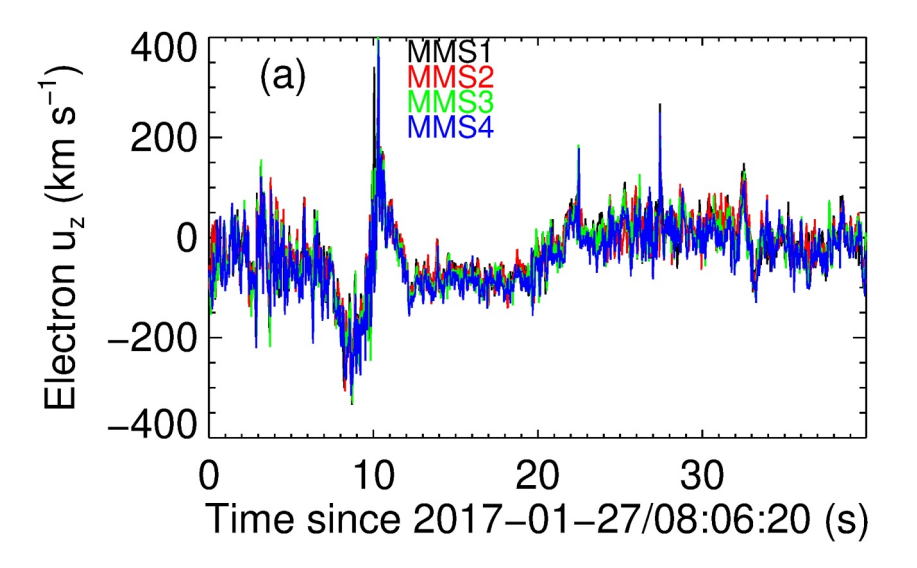
Table A1 *Mean and Standard Deviations of the Measured Ion and Electron Velocities Maesured by the Four MMS Spacecraft*

	$\langle u_x \rangle \pm \sigma_{u_x}$	$\langle u_y \rangle \pm \sigma_{u_y}$	$\langle u_z \rangle \pm \sigma_{u_z}$	$\langle u_x Er \rangle \pm \sigma_{u_x Er}$	$\langle u_y Er \rangle \pm \sigma_{u_y Er}$	$\langle u_z Er \rangle \pm \sigma_{u_z Er}$
MMS1 I	-279 ± 98	-140 ± 63	-48 ± 58	1.6 ± 0.4	1.9 ± 1.9	1.1 ± 0.3
MMS2 I	-280 ± 99	-141 ± 64	-50 ± 56	1.6 ± 0.4	2.0 ± 1.7	1.2 ± 0.3
MMS3 I	-278 ± 99	-141 ± 64	-48 ± 57	1.7 ± 0.4	2.0 ± 2.0	1.2 ± 0.2
MMS4 I	-280 ± 100	-140 ± 64	-48 ± 57	1.6 ± 0.4	2.2 ± 2.8	1.2 ± 0.3
MMS1 E	-260 ± 107	-132 ± 88	-29 ± 72	9.5 ± 1.0	12.4 ± 4.0	7.7 ± 1.8
MMS2 E	-257 ± 101	-130 ± 81	-27 ± 67	9.5 ± 0.9	12.2 ± 3.1	7.5 ± 1.4
MMS3 E	-262 ± 106	-132 ± 90	-35 ± 69	9.4 ± 0.9	11.9 ± 3.5	7.2 ± 1.7
MMS4 E	-263 ± 105	-132 ± 85	-43 ± 69	9.5 ± 0.9	12.0 ± 3.3	7.6 ± 1.3

Note. The mean and standard deviations of the reported statistical error is also given.

ROBERTS ET AL. 14 of 20

21699402, 2025, 11, Downloaded from https://agupub.son.linelibrary.wiley.com/doi/10.1029/2025/1A034141, Wiley Online Library on [21/11/2025]. See the Terms and Conditions (https://onlinelibrary.wiley.com/terms-and-conditions) on Wiley Online Library for rules of use; OA articles are governed by the applicable Creative Commons Licensea



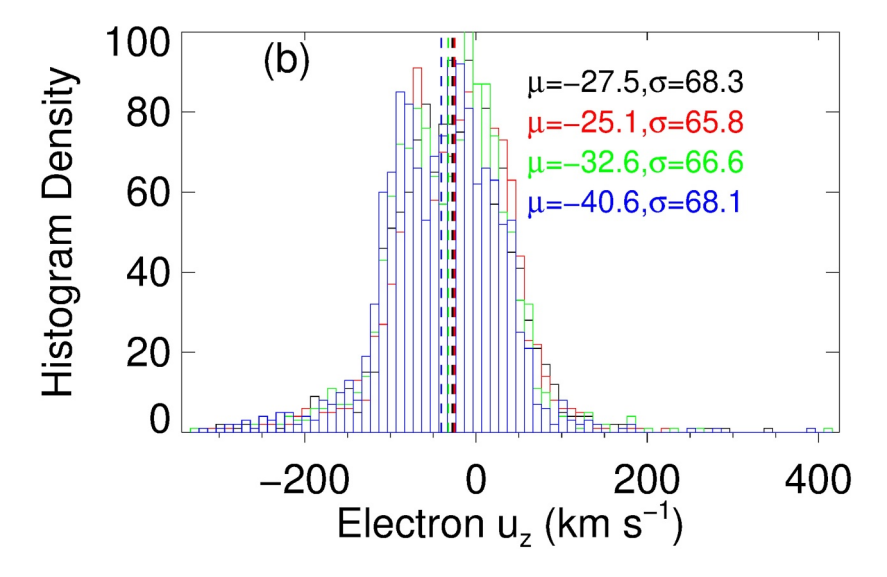


Figure A1. (a) Measured data from the four spacecraft for the u_z component of electron velocity. (b) Histogram of the data with the mean (μ) and standard deviations (σ) the dashed lines denote the mean values.

ROBERTS ET AL. 15 of 20

21699402, 2025, 11, Downloaded from https://agupubs.onlinelibrary.wiley.com/doi/10.1029/2025/A034414, Wiley Online Library on [21/11/2025]. See the Terms and Conditions

and-conditions) on Wiley Online Library for rules of use; OA articles are governed by the applicable Creative Commons Licenso

Acknowledgments

O.W.R and Z.V. thanks FWF project

the Austrian Science Fund (FWF): P

PAT9232923 and gratefully acknowledge

37265-N for supporting this project. O.W.

R, Z.V, F.K, and M.T acknowledge the

(FWF): P 33285-N. F.K. is supported by

X000974/1. S.R. acknowledges support by

80NSSC25K7353. C.S.W. thanks the

Austrian Science Fund (FWF) 10.55776/

support by the Austrian Science Fund

the STFC Consolidated Grant ST/

the MMS Early Career Award

support under Grant 10.55776/

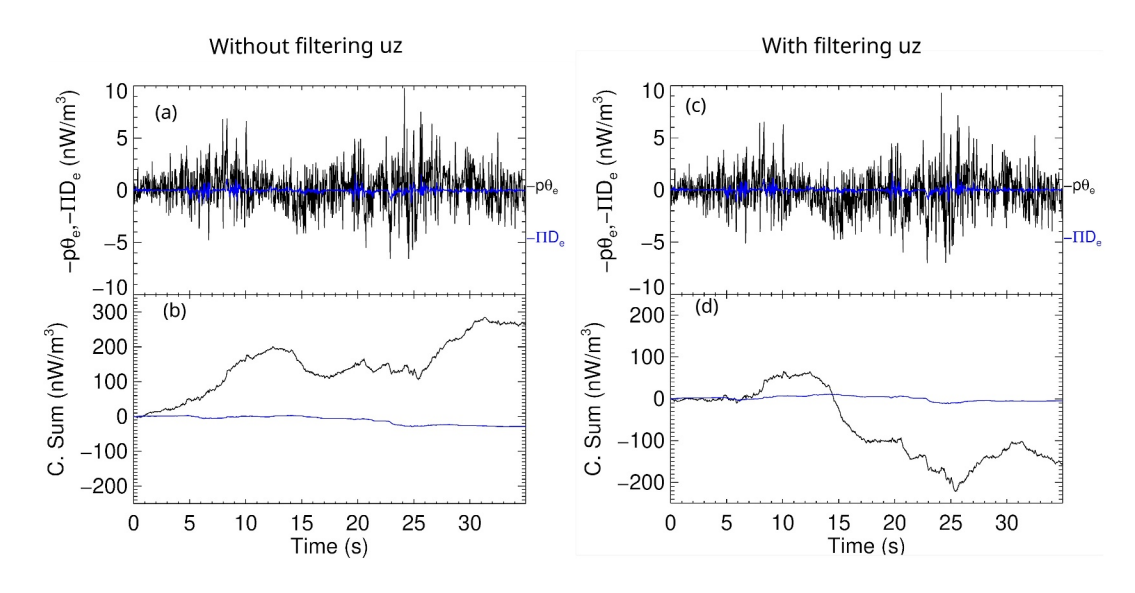


Figure A2. (a) Electron pressure strain terms and the cumulative sums (b) where the u_z component has not been filtered, (c, d) shows the same as (a, b) but the u_z component has been high pass filtered.

Conflict of Interest

The authors declare no conflicts of interest relevant to this study.

Data Availability Statement

The observational data are publicly available through the MMS Science Data Center (https://lasp.colorado.edu/mms/sdc/public/about).

References

Alexandrova, O. (2008). Solar wind vs magnetosheath turbulence and alfvén vortices. *Nonlinear Processes in Geophysics*, 15(1), 95–108. https://doi.org/10.5194/npg-15-95-2008

Angelopoulos, V. (2009). The themis mission. In *The themis mission* (pp. 5–34). Springer. https://doi.org/10.1007/978-0-387-89820-9_2 Archer, M. O., Horbury, T. S., & Eastwood, J. P. (2012). Magnetosheath pressure pulses: Generation downstream of the bow shock from solar

Archer, M. O., Horbury, T. S., & Eastwood, J. P. (2012). Magnetosheath pressure pulses: Generation downstream of the bow shock from solar wind discontinuities. *Journal of Geophysical Research*, 117(A5), 1–13. https://doi.org/10.1029/2011JA017468

Archer, M. O., Horbury, T. S., Eastwood, J. P., Weygand, J. M., & Yeoman, T. K. (2013). Magnetospheric response to magnetosheath pressure pulses: A low-pass filter effect. *Journal of Geophysical Research: Space Physics*, 118(9), 5454–5466. https://doi.org/10.1002/jgra.50519
 Archer, M. O., Turner, D. L., Eastwood, J. P., Horbury, T. S., & Schwartz, S. J. (2014). The role of pressure gradients in driving sunward magnetosheath flows and magnetopause motion. *Journal of Geophysical Research: Space Physics*, 119(10), 8117–8125. https://doi.org/10.

1002/2014/A020342

Argall, M. R., Fischer, D., Contel, O. L., Mirioni, L., Torbert, R. B., Dors, I., et al. (2018). The fluxgate-searchcoil merged (fsm) magnetic field

data product for mms. arXiv, 1-6.

Artemyev, A. V., Shi, C., Lin, Y., Nishimura, Y., Gonzalez, C., Verniero, J., et al. (2022). Ion kinetics of plasma flows: Earth's magnetosheath versus solar wind. The Astrophysical Journal, 939(2), 85. https://doi.org/10.3847/1538-4357/ac96e4

Bandyopadhyay, R., Chasapis, A., Chhiber, R., Parashar, T. N., Matthaeus, W. H., Shay, M. A., et al. (2018). Incompressive energy transfer in the earth's magnetosheath: Magnetospheric multiscale observations. *The Astrophysical Journal*, 866(2), 106. https://doi.org/10.3847/1538-4357/aade04

Bandyopadhyay, R., Chasapis, A., Matthaeus, W. H., Parashar, T. N., Haggerty, C. C., Shay, M. A., et al. (2021). Energy dissipation in turbulent reconnection. *Physics of Plasmas*, 28(11), 112305. https://doi.org/10.1063/5.0071015

Bandyopadhyay, R., Matthaeus, W. H., Parashar, T. N., Yang, Y., Chasapis, A., Giles, B. L., et al. (2020). Statistics of kinetic dissipation in the earth's magnetosheath: Mms observations. *Physical Review Letters*, 124(25), 255101. https://doi.org/10.1103/PhysRevLett.124.255101

Blanco-Cano, X., Preisser, L., Kajdič, P., & Rojas-Castillo, D. (2020). Magnetosheath microstructure: Mirror mode waves and jets during southward IP magnetic field. *Journal of Geophysical Research: Space Physics*, 125(9), e2020JA027940. https://doi.org/10.1029/2020JA027940

Blanco-Cano, X., Rojas-Castillo, D., Kajdič, P., & Preisser, L. (2023). Jets and mirror mode waves in earth's magnetosheath. *Journal of Geophysical Research: Space Physics*, 128(7), e2022JA031221, https://doi.org/10.1029/2022JA031221

Burch, J. L., Moore, T. E., Torbert, R. B., & Giles, B. L. (2016a). Magnetospheric multiscale overview and science objectives. Space Science Reviews, 199(1–4), 5–21. https://doi.org/10.1007/s11214-015-0164-9

Burch, J. L., Torbert, R. B., Phan, T. D., Chen, L. J., Moore, T. E., Ergun, R. E., et al. (2016b). Electron-scale measurements of magnetic reconnection in space. *Science*, 352(6290), aaf2939. https://doi.org/10.1126/science.aaf2939

Chanteur, G. (2000). Accuracy of fields gradient estimations by cluster: Explanation of its dependency upon elongation and planarity of the tetrahedron. In Cluster-ii workshop: Multiscale/multipoint plasma measurements. In *Proceedings of the workshop held at imperial college*, 265

ROBERTS ET AL. 16 of 20

- Chasapis, A., Matthaeus, W. H., Parashar, T. N., LeContel, O., Retinò, A., Breuillard, H., et al. (2017). Electron heating at kinetic scales in magnetosheath turbulence. *The Astrophysical Journal*, 836(2), 247. https://doi.org/10.3847/1538-4357/836/2/247
- Chasapis, A., Yang, Y., Matthaeus, W. H., Parashar, T. N., Haggerty, C. C., Burch, J. L., et al. (2018). Energy conversion and collisionless plasma dissipation channels in the turbulent magnetosheath observed by the magnetospheric multiscale mission. *The Astrophysical Journal*, 862(1), 32. https://doi.org/10.3847/1538-4357/aac775
- Chhiber, R., Chasapis, A., Bandyopadhyay, R., Parashar, T. N., Matthaeus, W. H., Maruca, B. A., et al. (2018). Higher-order turbulence statistics in the earth's magnetosheath and the solar wind using magnetospheric multiscale observations. *Journal of Geophysical Research: Space Physics*, 123(12), 9941–9954. https://doi.org/10.1029/2018JA025768
- Dmitriev, A. V., & Suvorova, A. V. (2012). Traveling magnetopause distortion related to a large-scale magnetosheath plasma jet: Themis and ground-based observations. *Journal of Geophysical Research*, 117(A8), 1–16. https://doi.org/10.1029/2011JA016861
- Dunlop, M., Southwood, D., Glassmeier, K.-H., & Neubauer, F. (1988). Analysis of multipoint magnetometer data. *Advances in Space Research*, 8(9–10), 273–277. https://doi.org/10.1016/0273-1177(88)90141-X
- Dunlop, M. W., Balogh, A., Glassmeier, K.-H., & Robert, P. (2002). Four-point cluster application of magnetic field analysis tools: The curl-ometer. *Journal of Geophysical Research*, 107(A11), 1–14. https://doi.org/10.1029/2001JA005088
- Dunlop, M. W., Dong, X. C., Wang, T. Y., Eastwood, J. P., Robert, P., Haaland, S., et al. (2021). Curlometer technique and applications. *Journal of Geophysical Research: Space Physics*, 126(11), e2021JA029538. https://doi.org/10.1029/2021JA029538
- Ergun, R. E., Goodrich, K. A., Wilder, F. D., Ahmadi, N., Holmes, J. C., Eriksson, S., et al. (2018). Magnetic reconnection, turbulence, and particle acceleration: Observations in the earth's magnetotail. *Geophysical Research Letters*, 45(8), 3338–3347. https://doi.org/10.1002/2018GL076993
- Ergun, R. E., Tucker, S., Westfall, J., Goodrich, K. A., Malaspina, D. M., Summers, D., et al. (2016). The axial double probe and fields signal processing for the mms mission. Space Science Reviews, 199(1–4), 167–188. https://doi.org/10.1007/s11214-014-0115-x
- Eriksson, E., Vaivads, A., Graham, D. B., Khotyaintsev, Y. V., Yordanova, E., Hietala, H., et al. (2016). Strong current sheet at a magnetosheath jet: Kinetic structure and electron acceleration. *Journal of Geophysical Research: Space Physics*, 121(10), 9608–9618. https://doi.org/10.1002/2016JA023146
- Escoubet, C. P., Hwang, K.-J., Toledo-Redondo, S., Turc, L., Haaland, S. E., Aunai, N., et al. (2020). Cluster and mms simultaneous observations of magnetosheath high speed jets and their impact on the magnetopause. *Frontiers in Astronomy and Space Sciences*, 6, 78. https://doi.org/10.3389/fspas.2019.00078
- Fargette, N., Lavraud, B., Rouillard, A. P., Houdayer, P. S., Phan, T. D., Øieroset, M., et al. (2023). Clustering of magnetic reconnection exhausts in the solar wind: An automated detection study. Astronomy and Astrophysics, 674, A98. https://doi.org/10.1051/0004-6361/202346043
- Fatemi, S., Hamrin, M., Krämer, E., Gunell, H., Nordin, G., Karlsson, T., & Goncharov, O. (2024). Unveiling the 3d structure of magnetosheath jets. *Monthly Notices of the Royal Astronomical Society*, 531(4), 4692–4713. https://doi.org/10.1093/mnras/stae1456
- Fischer, D., Magnes, W., Hagen, C., Dors, I., Chutter, M. W., Needell, J., et al. (2016). Optimized merging of search coil and fluxgate data for mms. Geoscientific Instrumentation, Methods and Data Systems, 5(2), 521–530. https://doi.org/10.5194/gi-5-521-2016
- Gershman, D. J., Avanov, L. A., Boardsen, S. A., Dorelli, J. C., Gliese, U., Barrie, A. C., et al. (2017). Spacecraft and instrument photoelectrons measured by the dual electron spectrometers on mms. *Journal of Geophysical Research: Space Physics*, 122(11), 11548–11558. https://doi.org/10.1002/2017JA024518
- Gershman, D. J., Dorelli, J. C., F.-Viñas, A., & Pollock, C. J. (2015). The calculation of moment uncertainties from velocity distribution functions with random errors. *Journal of Geophysical Research: Space Physics*, 120(8), 6633–6645. https://doi.org/10.1002/2014JA020775
- Gershman, D. J., F.-Viñas, A., Dorelli, J. C., Goldstein, M. L., Shuster, J., Avanov, L. A., et al. (2018). Energy partitioning constraints at kinetic scales in low- β turbulence. *Physics of Plasmas*, 25(2), 022303. https://doi.org/10.1063/1.5009158
- Graham, D. B., Khotyaintsev, Y. V., André, M., Vaivads, A., Chasapis, A., Matthaeus, W. H., et al. (2021). Non-maxwellianity of electron distributions near earth's magnetopause. *Journal of Geophysical Research: Space Physics*, 126(10), e2021JA029260. https://doi.org/10.1029/2021JA029260
- Greco, A., Valentini, F., Servidio, S., & Matthaeus, W. H. (2012). Inhomogeneous kinetic effects related to intermittent magnetic discontinuities. *Physical Review E*, 86, 1–6. https://doi.org/10.1103/PhysRevE.86.066405
- Gunell, H., Hamrin, M., Nesbit-Östman, S., Krämer, E., & Nilsson, H. (2023). Magnetosheath jets at Mars. Science Advances, 9(22), eadg5703. https://doi.org/10.1126/sciadv.adg5703
- Guo, J., Lu, S., Lu, Q., Ren, J., Ma, J., Slavin, J. A., et al. (2025). Three-dimensional global hybrid simulation of magnetosheath jets at Mercury. The Astrophysical Journal Letters, 978(1), L9. https://doi.org/10.3847/2041-8213/ad9dd7
- Gutynska, O., Sibeck, D. G., & Omidi, N. (2015). Magnetosheath plasma structures and their relation to foreshock processes. *Journal of Geophysical Research: Space Physics*, 120(9), 7687–7697. https://doi.org/10.1002/2014JA020880
- Han, D.-S., Liu, J.-J., Chen, X.-C., Xu, T., Li, B., Hu, Z.-J., et al. (2018). Direct evidence for throat Aurora being the ionospheric signature of magnetopause transient and reflecting localized magnetopause indentations. *Journal of Geophysical Research: Space Physics*, 123(4), 2658–2667. https://doi.org/10.1002/2017JA024945
- Hao, Y., Lembege, B., Lu, Q., & Guo, F. (2016). Formation of downstream high-speed jets by a rippled nonstationary quasi-parallel shock: 2-d hybrid simulations. *Journal of Geophysical Research: Space Physics*, 121(3), 2080–2094. https://doi.org/10.1002/2015JA021419
- Hietala, H., Laitinen, T. V., Andréeová, K., Vainio, R., Vaivads, A., Palmroth, M., et al. (2009). Supermagnetosonic jets behind a collisionless quasiparallel shock. *Physical Review Letters*, 103(24), 245001. https://doi.org/10.1103/PhysRevLett.103.245001
- Hietala, H., Phan, T. D., Angelopoulos, V., Oieroset, M., Archer, M. O., Karlsson, T., & Plaschke, F. (2018). In situ observations of a magnetosheath high-speed jet triggering magnetopause reconnection. *Geophysical Research Letters*, 45(4), 1732–1740. https://doi.org/10.1002/2017GL076525
- Karimabadi, H., Roytershteyn, V., Vu, H. X., Omelchenko, Y. A., Scudder, J., Daughton, W., et al. (2014). The link between shocks, turbulence, and magnetic reconnection in collisionless plasmas. *Physics of Plasmas*, 21(6), 062308. https://doi.org/10.1063/1.4882875
- Karlsson, T., Kullen, A., Liljeblad, E., Brenning, N., Nilsson, H., Gunell, H., & Hamrin, M. (2015). On the origin of magnetosheath plasmoids and their relation to magnetosheath jets. *Journal of Geophysical Research A: Space Physics*, 120(9), 7390–7403. https://doi.org/10.1002/2015JA021487
- Karlsson, T., Plaschke, F., Hietala, H., Archer, M., Blanco-Cano, X., Kajdič, P., et al. (2018). Investigating the anatomy of magnetosheath jets–Mms observations. *Annales Geophysicae*, 36(2), 655–677. https://doi.org/10.5194/angeo-36-655-2018
- Kaufmann, R. L., & Paterson, W. R. (2009). Boltzmann h function and entropy in the plasma sheet. Journal of Geophysical Research, 114(A9), A00D04. https://doi.org/10.1029/2008JA014030
- Khrabrov, A. V., & Sonnerup, B. U. (1998). Magnetic variance analysis for small-amplitude waves and flux transfer events on a current sheet. Journal of Geophysical Research, 103(A6), 11907–11918. https://doi.org/10.1029/98JA00615

ROBERTS ET AL. 17 of 20

- King, J. H., & Papitashvili, N. (2005). Solar wind spatial scales in and comparisons of hourly wind and ace plasma and magnetic field data. *Journal of Geophysical Research*, 110(A2), A02104. https://doi.org/10.1029/2004JA010649
- Koller, F., Plaschke, F., Temmer, M., Preisser, L., Roberts, O. W., & Vörös, Z. (2023). Magnetosheath jet formation influenced by parameters in solar wind structures. *Journal of Geophysical Research: Space Physics*, 128(4), 1–17. https://doi.org/10.1029/2023JA031339
- Koller, F., Temmer, M., Preisser, L., Plaschke, F., Geyer, P., Jian, L. K., et al. (2022). Magnetosheath jet occurrence rate in relation to CMES and sirs. Journal of Geophysical Research: Space Physics, 127(4), e2021JA030124. https://doi.org/10.1029/2021ja030124
- Krämer, E., Fatemi, S., Hamrin, M., Gunell, H., & Nordin, G. (2025a). On the kinetic energy input of magnetosheath jets into the magnetosheath. Geophysical Research Letters, 52(15), e2025GL115260. https://doi.org/10.1029/2025GL115260
- Krämer, E., Hamrin, M., Gunell, H., Karlsson, T., Steinvall, K., Goncharov, O., & André, M. (2023). Waves in magnetosheath Jets—Classification and the search for generation mechanisms using mms burst mode data. *Journal of Geophysical Research: Space Physics*, 128, 1–20. https://doi.org/10.1029/2023JA031621
- Krämer, E., Koller, F., Suni, J., LaMoury, A. T., Pöppelwerth, A., Glebe, G., et al. (2025b). Jets downstream of collisionless shocks: Recent discoveries and challenges. Space Science Reviews, 221(1), 4. https://doi.org/10.1007/s11214-024-01129-3
- LaMoury, A. T., Hietala, H., Plaschke, F., Vuorinen, L., & Eastwood, J. P. (2021). Solar wind control of magnetosheath jet formation and propagation to the magnetopause. *Journal of Geophysical Research: Space Physics*, 126(9), 1–15. https://doi.org/10.1029/2021JA029592
- Lindqvist, P.-A., Olsson, G., Torbert, R. B., King, B., Granoff, M., Rau, D., et al. (2016). The spin-plane double probe electric field instrument for mms. Space Science Reviews, 199(1–4), 137–165. https://doi.org/10.1007/s11214-014-0116-9
- Liu, H., Zong, Q. G., Zhang, H., Xiao, C. J., Shi, Q. Q., Yao, S. T., et al. (2019a). Mms observations of electron scale magnetic cavity embedded in proton scale magnetic cavity. *Nature Communications*, 10, 1–11. https://doi.org/10.1038/s41467-019-08971-y
- Liu, T. Z., Angelopoulos, V., Hietala, H., & III, L. B. W. (2017). Statistical study of particle acceleration in the core of foreshock transients. Journal of Geophysical Research: Space Physics, 122(7), 7197–7208. https://doi.org/10.1002/2017JA024043
- Liu, T. Z., Hietala, H., Angelopoulos, V., Omelchenko, Y., Roytershteyn, V., & Vainio, R. (2019b). Themis observations of particle acceleration by a magnetosheath jet-driven bow wave. *Geophysical Research Letters*, 46(14), 7929–7936. https://doi.org/10.1029/2019GL082614
- Liu, T. Z., Hietala, H., Angelopoulos, V., Omelchenko, Y., Vainio, R., & Plaschke, F. (2020a). Statistical study of magnetosheath jet-driven bow waves. *Journal of Geophysical Research: Space Physics*, 125(7), 1–14. https://doi.org/10.1029/2019JA027710
- Liu, T. Z., Hietala, H., Angelopoulos, V., Vainio, R., & Omelchenko, Y. (2020b). Electron acceleration by magnetosheath jet-driven bow waves. Journal of Geophysical Research: Space Physics, 125(7), 1–13. https://doi.org/10.1029/2019JA027709
- Liu, T. Z., Lu, S., Angelopoulos, V., Lin, Y., & Wang, X. Y. (2018). Ion acceleration inside foreshock transients. *Journal of Geophysical*
- Research: Space Physics, 123(1), 163–178. https://doi.org/10.1002/2017JA024838

 Lucek, E. A., Constantinescu, D., Goldstein, M. L., Pickett, J., Pinçon, J. L., Sahraoui, F., et al. (2005). The magnetosheath. Space Science
- Lucek, E. A., Constantinescu, D., Goldstein, M. L., Pickett, J., Pinçon, J. L., Sahraoui, F., et al. (2005). The magnetosheath. *Space Scienc Reviews*, 118(1–4), 95–152. https://doi.org/10.1007/s11214-005-3825-2
- Narita, Y., Plaschke, F., & Vörös, Z. (2021). In The magnetosheath, (pp. 137-152). https://doi.org/10.1002/9781119815624.ch9
- Němeček, Z., Šafránková, J., Přech, L., Sibeck, D. G., Kokubun, S., & Mukai, T. (1998). Transient flux enhancements in the magnetosheath. Geophysical Research Letters, 25(8), 1273–1276. https://doi.org/10.1029/98GL50873
- Ng, J., Chen, L. J., & Omelchenko, Y. A. (2021). Bursty magnetic reconnection at the earth's magnetopause triggered by high-speed jets. *Physics of Plasmas*, 28(9), 092902. https://doi.org/10.1063/5.0054394
- Norenius, L., Hamrin, M., Goncharov, O., Gunell, H., Opgenoorth, H., Pitkänen, T., et al. (2021). Ground-based magnetometer response to impacting magnetosheath jets. *Journal of Geophysical Research: Space Physics*, 126(8), e2021JA029115. https://doi.org/10.1029/2021JA029115
- Nykyri, K., Bengtson, M., Angelopoulos, V., Nishimura, Y., & Wing, S. (2019). Can enhanced flux loading by high-speed jets lead to a substorm? Multipoint detection of the christmas day substorm onset at 08:17 ut, 2015. *Journal of Geophysical Research: Space Physics*, 124(6), 4314–4340. https://doi.org/10.1029/2018JA026357
- Omelchenko, Y. A., Chen, L. J., & Ng, J. (2021). 3d space-time adaptive hybrid simulations of magnetosheath high-speed jets. *Journal of Geophysical Research: Space Physics*, 126(7), e2020JA029035. https://doi.org/10.1029/2020JA029035
- Palmroth, M., Hietala, H., Plaschke, F., Archer, M., Karlsson, T., Blanco-Cano, X., et al. (2018). Magnetosheath jet properties and evolution as determined by a global hybrid-vlasov simulation. *Annales Geophysicae*, 36(5), 1171–1182. https://doi.org/10.5194/angeo-36-1171-2018
- Palmroth, M., Raptis, S., Suni, J., Karlsson, T., Turc, L., Johlander, A., et al. (2021). Magnetosheath jet evolution as a function of lifetime: Global hybrid-vlasov simulations compared to mms observations. *Annales Geophysicae*, 39(2), 289–308. https://doi.org/10.5194/angeo-39-289-2021
 Paschmann, G. (1998). In G. Paschmann (Ed.), *Analysis methods for multi-spacecraft data*. Retrieved from http://scholar.google.com/scholar?
 - hl=en&btnG=Search&q=intitle:Analysis+Methods+for+Multi-Spacecraft+Data#1
- Paschmann, G., & Daly, P. (2008). In Multi-spacecraft analysis methods revisited. Retrieved from http://adsabs.harvard.edu/abs/2008msam.book
 Perri, S., Perrone, D., Yordanova, E., Sorriso-Valvo, L., Paterson, W. R., Gershman, D. J., et al. (2020). On the deviation from maxwellian of the ion velocity distribution functions in the turbulent magnetosheath. Journal of Plasma Physics, 86(1), 905860108. https://doi.org/10.1017/S0022377820000021
- Perrone, D., Settino, A., Perri, S., D'Amicis, R., Marco, R. D., Nicolaou, G., et al. (2024). Solar orbiter observations of proton and alpha particle kinetic signatures related to the presence of switchbacks in the inner heliosphere: A case study. *The Astrophysical Journal*, 973(2), 171. https://doi.org/10.3847/1538-4357/ad65db
- Pezzi, O., Liang, H., Juno, J. L., Cassak, P. A., Vásconez, C. L., Sorriso-Valvo, L., et al. (2021). Dissipation measures in weakly collisional plasmas. *Monthly Notices of the Royal Astronomical Society*, 505(4), 4857–4873. https://doi.org/10.1093/mnras/stab1516
- Pezzi, O., Yang, Y., Valentini, F., Servidio, S., Chasapis, A., Matthaeus, W. H., & Veltri, P. (2019). Energy conversion in turbulent weakly collisional plasmas: Eulerian hybrid vlasov-maxwell simulations. *Physics of Plasmas*, 26(7), 1–11. https://doi.org/10.1063/1.5100125
- Phan, T. D., Eastwood, J. P., Shay, M. A., Drake, J. F., Sonnerup, B. U., Fujimoto, M., et al. (2018). Electron magnetic reconnection without ion coupling in earth's turbulent magnetosheath. *Nature*, 557(7704), 202–206. https://doi.org/10.1038/s41586-018-0091-5
- Plaschke, F., Hietala, H., Archer, M., Blanco-Cano, X., Kajdič, P., Karlsson, T., et al. (2018). Jets downstream of collisionless shocks. *Space Science Reviews*, 214(5), 81. https://doi.org/10.1007/s11214-018-0516-3
- Plaschke, F., Hietala, H., & Vörös, Z. (2020). Scale sizes of magnetosheath jets. *Journal of Geophysical Research: Space Physics*, 125, 1–18. https://doi.org/10.1029/2020JA027962
- Plaschke, F., Hietala, H., & Angelopoulos, V. (2013). Anti-sunward high-speed jets in the subsolar magnetosheath. *Annales Geophysicae*, 31(10), 1877–1889. https://doi.org/10.5194/angeo-31-1877-2013
- Pollock, C., Moore, T., Jacques, A., Burch, J., Gliese, U., Saito, Y., et al. (2016). Fast plasma investigation for magnetospheric multiscale. Space Science Reviews, 199(1–4), 331–406. https://doi.org/10.1007/s11214-016-0245-4

ROBERTS ET AL. 18 of 20

- Preisser, L., Blanco-Cano, X., Kajdič, P., Burgess, D., & Trotta, D. (2020). Magnetosheath jets and plasmoids: Characteristics and formation mechanisms from hybrid simulations. *The Astrophysical Journal Letters*, 900(1), L6. https://doi.org/10.3847/2041-8213/abad2b
- Raptis, S., Karlsson, T., Plaschke, F., Kullen, A., & Lindqvist, P. (2020). Classifying magnetosheath jets using mms: Statistical properties. *Journal of Geophysical Research: Space Physics*, 125(11), e2019JA027754. https://doi.org/10.1029/2019JA027754
- Raptis, S., Karlsson, T., Vaivads, A., Pollock, C., Plaschke, F., Johlander, A., et al. (2022). Downstream high-speed plasma jet generation as a direct consequence of shock reformation. *Nature Communications*, 13(1), 598. https://doi.org/10.1038/s41467-022-28110-4
- Raptis, S., Lalti, A., Lindberg, M., Turner, D. L., Caprioli, D., & Burch, J. L. (2025a). Revealing an unexpectedly low electron injection threshold via reinforced shock acceleration. *Nature Communications*, 16(1), 488. https://doi.org/10.1038/s41467-024-55641-9
- Raptis, S., Lindberg, M., Liu, T. Z., Turner, D. L., Lalti, A., Zhou, Y., et al. (2025b). Multimission observations of relativistic electrons and high-speed jets linked to shock-generated transients. *The Astrophysical Journal Letters*, 981(1), L10. https://doi.org/10.3847/2041-8213/adb154
- Ren, J., Guo, J., Lu, Q., Lu, S., Gao, X., Ma, J., & Wang, R. (2024). Honeycomb-like magnetosheath structure formed by jets: Three-dimensional global hybrid simulations. *Geophysical Research Letters*, 51(12), e2024GL109925. https://doi.org/10.1029/2024GL109925
- Retinò, A., Sundkvist, D., Vaivads, A., & Mozer, F. (2007). In situ evidence of magnetic reconnection in turbulent plasma. *Nature Physics*. Retrieved from http://www.nature.com/nphys/journal/v3/n4/abs/nphys574.html
- Richard, L., Servidio, S., Svenningsson, I., Artemyev, A. V., Klein, K. G., Yordanova, E., et al. (2025). Non-maxwellianity of ion velocity distributions in the earth's magnetosheath. *Physical Review E*, 112(5), L053201. https://doi.org/10.1103/7p1x-84y9
- Robert, P., Roux, A., Harvey, C., Dunlop, M., Daly, P., & Glassmeier, K.-H. (1998). Tetrahedron geometric factors. In G. D. P Paschmann (Ed.) (pp. 323–348). *Analysis methods for multi-spacecraft data*
- Roberts, O. W., Narita, Y., Nakamura, R., & Vörös, Z. (2023). Spectral break of the density power spectrum in solar wind turbulence. Astronomy and Astrophysics, 677, L16. https://doi.org/10.1051/0004-6361/202346709
- Roberts, O. W., Narita, Y., Nakamura, R., Vörös, Z., & Gershman, D. (2019). Anisotropy of the spectral index in ion scale compressible turbulence: Mms observations in the magnetosheath. Frontiers in Physics. 7, 1–16. https://doi.org/10.3389/fphy.2019.00184
- bulence: Mms observations in the magnetosheath. Frontiers in Physics, 7, 1–16. https://doi.org/10.3389/fphy.2019.00184
 Roberts, O. W., Narita, Y., Nakamura, R., Vörös, Z., & Verscharen, D. (2022). The kinetic alfvén-like nature of turbulent fluctuations in the
- earth's magnetosheath: Mms measurement of the electron alfvén ratio. *Physics of Plasmas*, 29(1), 012308. https://doi.org/10.1063/5.0068828 Roberts, O. W., Toledo-Redondo, S., Perrone, D., Zhao, J., Narita, Y., Gershman, D., et al. (2018). Ion-scale kinetic alfvén turbulence: Mms
- measurements of the alfvén ratio in the magnetosheath. *Geophysical Research Letters*, 45, 7974–7984. https://doi.org/10.1029/2018GL078498 Russell, C. T., Anderson, B. J., Baumjohann, W., Bromund, K. R., Dearborn, D., Fischer, D., et al. (2016). The magnetospheric multiscale magnetometers. *Space Science Reviews*, 199(1–4), 189–256. https://doi.org/10.1007/s11214-014-0057-3
- Sarto, D. D., & Pegoraro, F. (2018). Shear-induced pressure anisotropization and correlation with fluid vorticity in a low collisionality plasma. Monthly Notices of the Royal Astronomical Society, 475(1), 181–192. https://doi.org/10.1093/mnras/stx3083
- Sarto, D. D., Pegoraro, F., & Califano, F. (2016). Pressure anisotropy and small spatial scales induced by velocity shear. *Physical Review E*, 93(5), 053203. https://doi.org/10.1103/PhysRevE.93.053203
- Servidio, S., Chasapis, A., Matthaeus, W. H., Perrone, D., Valentini, F., Parashar, T. N., et al. (2017). Magnetospheric multiscale observation of plasma velocity-space Cascade: Hermite representation and theory. *Physical Review Letters*, 119(20), 205101. https://doi.org/10.1103/PhysRevLett.119.205101
- Settino, A., Perrone, D., Khotyaintsev, Y. V., Graham, D. B., & Valentini, F. (2021). Kinetic features for the identification of kelvin–helmholtz vortices in in situ observations. *The Astrophysical Journal*, 912(2), 154. https://doi.org/10.3847/1538-4357/abf1f5
- Sonnerup, B. U., & Scheible, M. (1998). Minimum and maximum variance analysis. In Analysis methods for multi-spacecraft data.
- Tinoco-Arenas, A., Kajdič, P., Preisser, L., Blanco-Cano, X., Trotta, D., & Burgess, D. (2022). Parametric study of magnetosheath jets in 2d local hybrid simulations. Frontiers in Astronomy and Space Sciences, 9, 1–14. https://doi.org/10.3389/fspas.2022.793195
- Torbert, R. B., Burch, J. L., Phan, T. D., Hesse, M., Argall, M. R., Shuster, J., et al. (2018). Electron-scale dynamics of the diffusion region during symmetric magnetic reconnection in space. *Science*, 362(6421), 1391–1395. https://doi.org/10.1126/science.aat2998
- Turc, L., Roberts, O. W., Archer, M. O., Palmroth, M., Battarbee, M., Brito, T., et al. (2019). First observations of the disruption of the earth's foreshock wave field during magnetic clouds. *Geophysical Research Letters*, 46(22), 12644–12653. https://doi.org/10.1029/2019GL084437
- Turc, L., Roberts, O. W., Verscharen, D., Dimmock, A. P., Kajdič, P., Palmroth, M., et al. (2023). Transmission of foreshock waves through earth's bow shock. *Nature Physics*, 19(1), 78–86. https://doi.org/10.1038/s41567-022-01837-z
- Vörös, Z., Roberts, O. W., Yordanova, E., Sorriso-Valvo, L., Nakamura, R., Narita, Y., et al. (2023). How to improve our understanding of solar wind-magnetosphere interactions on the basis of the statistical evaluation of the energy budget in the magnetosheath? Frontiers in. Astronomy and Space Sciences, 10, 1–8. https://doi.org/10.3389/fspas.2023.1163139
- Vörös, Z., Yordanova, E., Echim, M. M., Consolini, G., & Narita, Y. (2016). Turbulence-generated proton-scale structures in the terrestrial magnetosheath. The Astrophysical Journal Letters, 819(1), L15. https://doi.org/10.3847/2041-8205/819/1/L15
- Vörös, Z., Yordanova, E., Varsani, A., Genestreti, K. J., Khotyaintsev, Y. V., Li, W., et al. (2017). Mms observation of magnetic reconnection in the turbulent magnetosheath. *Journal of Geophysical Research: Space Physics*, 122(11), 11442–11467. https://doi.org/10.1002/2017JA024535
- Vuorinen, L., Hietala, H., & Plaschke, F. (2019). Jets in the magnetosheath: Imf control of where they occur. *Annales Geophysicae*, 37(4), 689–697. https://doi.org/10.5194/angeo-37-689-2019
- Vuorinen, L., Vainio, R., Hietala, H., & Liu, T. Z. (2022). Monte carlo simulations of electron acceleration at bow waves driven by fast jets in the earth's magnetosheath. *The Astrophysical Journal*, 934(2), 165. https://doi.org/10.3847/1538-4357/ac7f42
- Wang, B., Nishimura, Y., Hietala, H., & Angelopoulos, V. (2022). Investigating the role of magnetosheath high-speed jets in triggering dayside ground magnetic ultra-low frequency waves. Geophysical Research Letters, 49(22), 1–11. https://doi.org/10.1029/2022GL099768
- Wang, B., Nishimura, Y., Hietala, H., Lyons, L., Angelopoulos, V., Plaschke, F., et al. (2018). Impacts of magnetosheath high-speed jets on the magnetosphere and ionosphere measured by optical imaging and satellite observations. *Journal of Geophysical Research: Space Physics*, 123(6), 4879–4894. https://doi.org/10.1029/2017JA024954
- Wilson, L. B., Sibeck, D. G., Breneman, A. W., Contel, O. L., Cully, C., Turner, D. L., et al. (2014a). Quantified energy dissipation rates in the terrestrial bow shock: 1. Analysis techniques and methodology. *Journal of Geophysical Research: Space Physics*, 119(8), 6455–6474. https://doi.org/10.1002/2014ja019929
- Wilson, L. B., Sibeck, D. G., Breneman, A. W., Contel, O. L., Cully, C., Turner, D. L., et al. (2014b). Quantified energy dissipation rates in the terrestrial bow shock: 2. Waves and dissipation. *Journal of Geophysical Research: Space Physics*, 119(8), 6475–6495. https://doi.org/10.1002/ 2014ja019930
- Yang, Y., Matthaeus, W. H., Parashar, T. N., Haggerty, C. C., Roytershteyn, V., Daughton, W., et al. (2017a). Energy transfer, pressure tensor, and heating of kinetic plasma. *Physics of Plasmas*, 24(7), 072306. https://doi.org/10.1063/1.4990421
- Yang, Y., Matthaeus, W. H., Parashar, T. N., Wu, P., Wan, M., Shi, Y., et al. (2017b). Energy transfer channels and turbulence Cascade in vlasov-maxwell turbulence. *Physical Review E*, 95(6), 061201. https://doi.org/10.1103/PhysRevE.95.061201

ROBERTS ET AL. 19 of 20



Journal of Geophysical Research: Space Physics

- 10.1029/2025JA034414
- Yang, Y., Matthaeus, W. H., Roy, S., Roytershteyn, V., Parashar, T. N., Bandyopadhyay, R., & Wan, M. (2022). Pressure–strain interaction as the energy dissipation estimate in collisionless plasma. *The Astrophysical Journal*, 929(2), 142. https://doi.org/10.3847/1538-4357/ac5d3e
- Yordanova, E., Vörös, Z., Varsani, A., Graham, D. B., Norgren, C., Khotyaintsev, Y. V., et al. (2016). Electron scale structures and magnetic reconnection signatures in the turbulent magnetosheath. *Geophysical Research Letters*, 43(12), 5969–5978. https://doi.org/10.1002/2016GL069191
- Zenitani, S., Hesse, M., Klimas, A., & Kuznetsova, M. (2011). New measure of the dissipation region in collisionless magnetic reconnection. *Physical Review Letters*, 106(19), 195003. https://doi.org/10.1103/PhysRevLett.106.195003
- Zenitani, S., Shinohara, I., & Nagai, T. (2012). Evidence for the dissipation region in magnetotail reconnection. *Geophysical Research Letters*, 39(11), 0–4. https://doi.org/10.1029/2012GL051938
- Zhang, H., Zong, Q., Connor, H., Delamere, P., Facskó, G., Han, D., et al. (2022). Dayside transient phenomena and their impact on the magnetosphere and ionosphere. *Author*, 218(5), 40. https://doi.org/10.1007/s11214-021-00865-0
- Zhou, Y., Raptis, S., Wang, S., Shen, C., Ren, N., & Ma, L. (2024). Magnetosheath jets at Jupiter and across the solar system. *Nature Communications*, 15(1), 4. https://doi.org/10.1038/s41467-023-43942-4
- Zhou, Y., Shen, C., & Ji, Y. (2023). Undulated shock surface formed after a shock–discontinuity interaction. *Geophysical Research Letters*, 50(10), e2023GL103848. https://doi.org/10.1029/2023GL103848

ROBERTS ET AL. 20 of 20